Palaeoposition of the Seychelles microcontinent in relation to the Deccan Traps and the Plume Generation Zone in Late Cretaceous-Early Palaeogene time

M. Ganerød, T. H. Torsvik, D. J. J. van Hinsbergen, et al.

Geological Society, London, Special Publications 2011; v. 357; p. 229-252
doi: 10.1144/SP357.12

Palaeoposition of the Seychelles microcontinent in relation to the Deccan Traps and the Plume Generation Zone in Late Cretaceous–Early Palaeogene time

M. GANERØD[1]*, T. H. TORSVIK[1,2,3], D. J. J. VAN HINSBERGEN[2,3], C. GAINA[1,2,3], F. CORFU[4], S. WERNER[2], T. M. OWEN-SMITH[5], L. D. ASHWAL[5], S. J. WEBB[5] & B. W. H. HENDRIKS[1]

[1]*Geodynamikk, Geological Survey of Norway, NO-7491 Trondheim, Norway*

[2]*Physics of Geological Processes (PGP), University of Oslo, P.O. Box 1048, Blindern, NO-0316 Oslo, Norway*

[3]*Center for Advanced Studies, Norwegian Academy of Science and Letters, Drammensveien 78, NO-0271 Oslo, Norway*

[4]*Department of Geosciences, University of Oslo, Pb 1047 Blindern, NO-0316 Oslo, Norway*

[5]*School of Geosciences, University of the Witwatersrand, Private Bag 3, Wits 2050, Johannesburg, South Africa*

**Corresponding author (e-mail: morgan.ganerod@ngu.no)*

Abstract: The Early Palaeogene magmatic rocks of North and Silhouette Islands in the Seychelles contain clues to the Cenozoic geodynamic puzzle of the Indian Ocean, but have so far lacked precise geochronological data and palaeomagnetic constraints. New $^{40}Ar/^{39}Ar$ and U–Pb dates demonstrate that these rocks were emplaced during magnetochron C28n; however, $^{40}Ar/^{39}Ar$ and palaeomagnetic data from Silhouette indicate that this complex experienced a protracted period of cooling. The Seychelles palaeomagnetic pole (57.55°S and 114.22°E; A9512.3°, $N = 14$) corresponds to poles of similar ages from the Deccan Traps after being corrected for a clockwise rotation of $29.4° \pm 12.9°$. This implies that Seychelles acted as an independent microplate between the Indian and African plates during and possibly after C27r time, confirming recent results based on kinematic studies. Our reconstruction confirms that the eruption of the Deccan Traps, which affected both India and the Seychelles and triggered continental break-up, can be linked to the present active Reunion hotspot, which is being sourced as a deep plume from the Plume Generation Zone.

Supplementary material: Experimental data are available at http://www.geolsoc.org.uk/SUP18482.

The late Mesozoic and Cenozoic northwards drift of the Indian plate was accommodated by subduction of the Neotethys Ocean below the Eurasian margin and the opening of the Indian Ocean to the south. The Indian Ocean comprises several sub-basins and intervening continental fragments that originated from Gondwana and were stranded by several events of spreading ridge relocation (McKenzie & Sclater 1971; Norton & Sclater 1979; Barron & Harrison 1980; Plummer & Belle 1995). Among these continental fragments is the Seychelles microcontinent, which is an almost entirely submerged and elongated continental fragment (Fig. 1) in the central part of the Indian Ocean (Baker 1963). The timing of separation of the Seychelles continent from India is documented by seafloor spreading along the Carlsberg Ridge (Fig. 1), where spreading anomalies correspond to chron C28n (64.1 Ma, according to GST2004 by Ogg & Smith 2004) and younger (Chaubey *et al.* 2002; Royer *et al.* 2002; Collier *et al.* 2008).

The Seychelles islands mainly expose coral reefs overlying undeformed Neoproterozoic granites (Velain 1879; Baker 1963), most of which fall within a 755–748 Ma age window (U–Pb; Tucker *et al.* 2001). However, on the islands of Silhouette and the North Island (Fig. 2), Late Cretaceous to Palaeogene alkaline central complexes and mafic volcanic rocks are exposed. These may correspond to the Late Cretaceous–Palaeogene Deccan Traps (Fig. 1), one of the most voluminous of the Large Igneous Provinces (Coffin & Eldholm 1992;

From: Van Hinsbergen, D. J. J., Buiter, S. J. H., Torsvik, T. H., Gaina, C. & Webb, S. J. (eds) *The Formation and Evolution of Africa: A Synopsis of 3.8 Ga of Earth History*. Geological Society, London, Special Publications, **357**, 229–252. DOI: 10.1144/SP357.12 0305-8719/11/$15.00

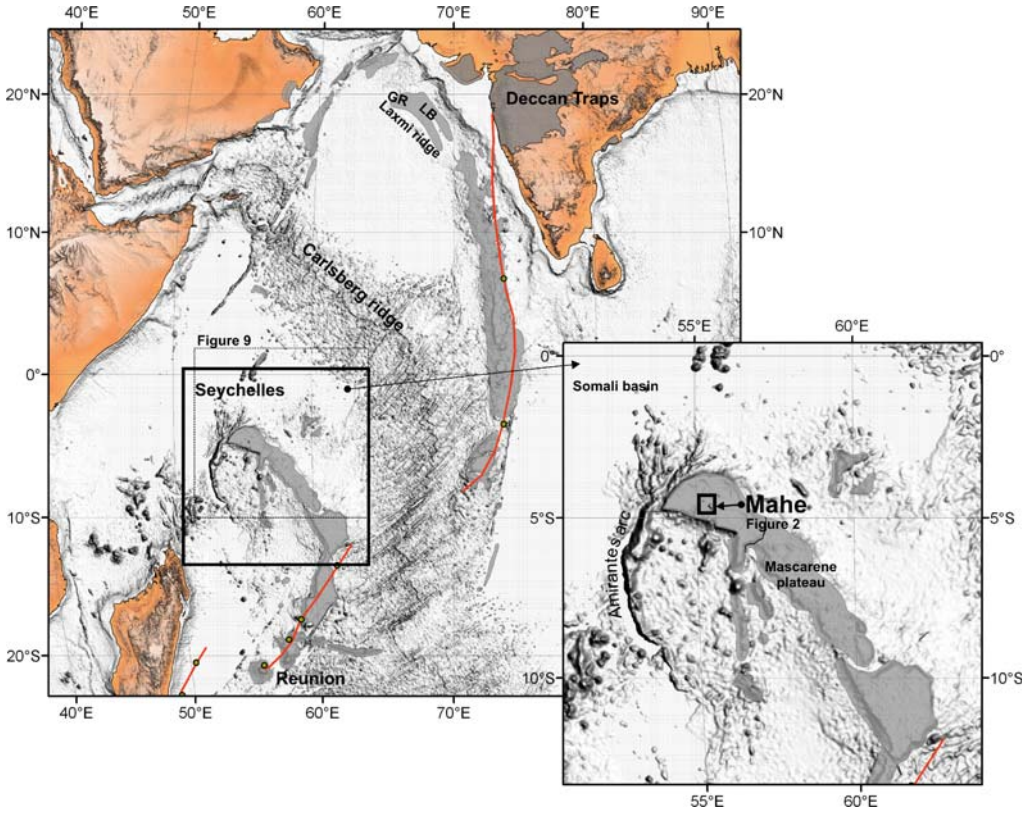

Fig. 1. Location of the Deccan Traps and the Seychelles. The proposed Reunion hotspot track of Duncan (1990) is shown in red. LB and GR denote Laxmi Basin and Gop Rift, respectively. The bathymetry and topography is produced from Smith & Sandwell (1997).

Courtillot *et al.* 1999) where Jay & Widdowson (2008) have provided an estimate of the original Deccan eruptive volume of *c.* 1.3×10^6 km^3. Deccan magmatism has been postulated to be associated with the separation of India from the Seychelles, after which the Seychelles effectively became reunited with the African plate. Establishing high-resolution age control of the mafic volcanics is therefore essential to determine whether volcanism related to the Deccan Traps occurred on both the Indian and Seychelles continents, and whether it was restricted to the Indian Subcontinent.

In order to address this issue we sampled the Late Cretaceous–Palaeogene successions on the Seychelles and carried out $^{40}Ar/^{39}Ar$ and U–Pb analyses. Additionally, we carried out a palaeomagnetic study to test whether the Seychelles and the Indian Deccan Traps share a common palaeomagnetic pole after correcting for younger sea-floor spreading. We use this information to reconstruct the palaeoposition of the Deccan Traps with respect to the African Large Low Shear-wave Velocity Province (LLSVP) at the core–mantle boundary, which has been referred to a Plume Generation Zone (Burke & Torsvik 2004; Burke *et al.* 2008; Torsvik *et al.* 2008*a*).

Geological setting

Opening of the Indian Ocean

During the Mid-Jurassic, Africa separated from East Antarctica and adjacent India–Seychelles–Madagascar forming the East Somali and Mozambique basins (Coffin & Rabinowitz 1988; König & Jokat 2006). Around the Mid-Cretaceous, Indian–Seychelles–Madagascar separated away from East Antarctica and Australia. Ever since, the Indian–Seychelles–Madagascar trio had a protracted history of rifting and drifting (e.g. Gaina *et al.* 2007). After passing over the assumed 'Marion hotspot' (Mahoney *et al.* 1991; Storey *et al.* 1995, 1997; Torsvik *et al.* 1998), India and the Seychelles drifted away from Madagascar, accommodated by

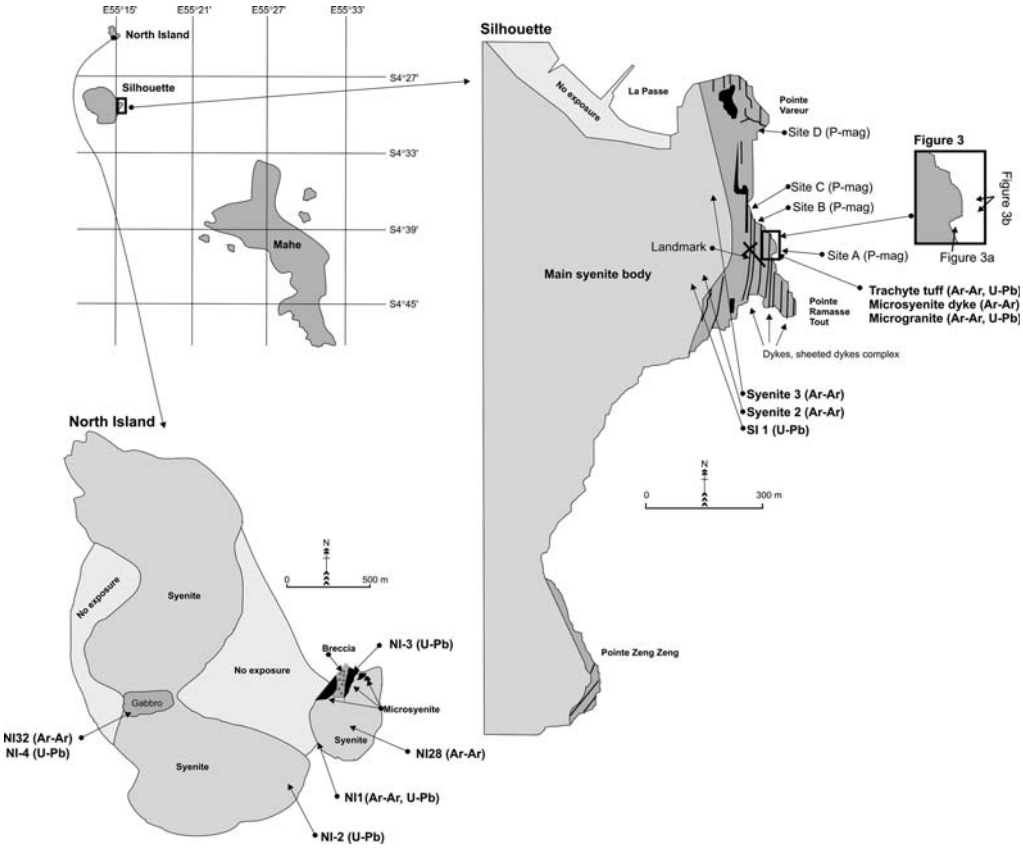

Fig. 2. The location of Silhouette and North Island. Silhouette, the palaeomagnetic sampling sites are divided into sites A–D; most sites measurements were made at site A. Samples for geochronological analysis from Silhouette are the syenite 2 and 3; the trachyte tuff, microsyenite dyke and the microgranite are taken from site A. North Island, samples for geochronologic analysis are the syenite samples NI1, NI28 and the NI32 gabbro. Modified from Stephens & Devey (1992).

the Mascarene spreading ridge. The separation was associated with widespread volcanism between 91.6 and 83.6 Ma, remnants of which are preserved in Madagascar (Storey *et al.* 1995; Torsvik *et al.* 1998). An anticlockwise rotation of the India–Seychelles platform has been proposed for this time window (Plummer 1995; Plummer & Belle 1995). Moving northwards, the impingement of the Réunion mantle plume in the Latest Cretaceous caused massive volcanism in Western India, known as the Deccan Traps. Around the same time, the mid-ocean ridge from the Mascarene Basin gradually relocated northwards between India and Seychelles to become the Carlsberg ridge (e.g. Royer *et al.* 2002), although the plume involvement in this scenario has been questioned (Sheth 2005). This event parted the Indian continent from the Seychelles (Duncan 1990). As a result of this history, microcontinental fragments derived from Gondwana are now widely distributed across the Indian Ocean. The present-day margin of West India has been described as a conglomerate of highly extended continental crust (Subrahmanyam *et al.* 1995) and small oceanic basins – such as the Gop Rift and possibly the Laxmi Basin (Krishna *et al.* 2006; Collier *et al.* 2008; Yatheesh *et al.* 2009) – that have been affected by volcanism (Deccan and possible pre-Deccan) and underplating (Lane 2006; Minshull *et al.* 2008) and formed several volcanic ridges (Calvès *et al.* 2008, 2011).

Age of the Deccan Traps

The age and the palaeomagnetic signature of the Deccan Traps have been a focus of research for several decades (e.g. Wensink 1973; Wensink *et al.* 1977). The earliest manifestations of Deccan volcanism are alkaline volcanic and intrusive

complexes in extensional areas north of the main Deccan province, dated at 68.5 ± 0.16 Ma (Basu *et al.* 1993). The culmination of emplacement of these complexes coincided with the onset of the voluminous tholeiitic Deccan volcanism. The first products of the Deccan flood basalts can be found in the north (Kutch region) and are dated at 67 Ma, whereas the most voluminous phase corresponds broadly in time with the K–T boundary at 65.5 Ma (Allègre *et al.* 1999; Courtillot *et al.* 1999; Courtillot & Renne 2003; Chenet *et al.* 2007), spanning magnetochron 29r and 29n (Jay *et al.* 2009) of the geomagnetic polarity timescale (Ogg & Smith 2004). Based on geochemical and geochronological evidence, a correlation of the Deccan to the Rajahmundry traps (SE India) was proposed (Self *et al.* 2008), dated 64.7 ± 0.57 Ma (Baksi 2005). Due to relative southwards migration of the eruptive centres, the geometry of each pulse has been described as consisting of large-scale clinoforms (e.g. Mitchell & Widdowson 1991). The culmination of the Deccan volcanism can be seen as trachytes in the western Indian rifted continental margin dated *c.* 61.5 ± 0.3 Ma (Sheth *et al.* 2001). This last phase of volcanism has also been documented in the conjugate Seychelles rift margin, as offshore seaward-dipping reflectors (Collier *et al.* 2008).

Geology of the Seychelles

The geology of the Seychelles is dominated by undeformed Neoproterozoic granitic rocks and dolerite dykes (Baker 1963; Ashwal *et al.* 2002) with ages between 755 and 748 Ma (Tucker *et al.* 2001). Paleocene alkaline igneous complexes are restricted to the Silhouette and North Islands (Fig. 2). Most of Silhouette consists of a body of syenite and a small unit of granite (Dickin *et al.* 1986).

On the eastern part of the Silhouette Island (from Pointe Zeng Zeng to Pointe Vareur, Fig. 2) a complex of trachytic tuff units, several pale-coloured microsyenite sheeted dykes, mafic dykes and microgranite dykes are exposed. The lavas contain fragments of syenite and older trachyte tuff, whereas the microsyenite sheeted dykes entrain fragments of trachyte. Two mafic dykes cut the complex close to Pointe Vareur, and are themselves cut by veins of granite (microgranite). Larger granite intrusions are also identified closer to Pointe Ramasse Tout. The trachyte tuffs were therefore emplaced first, followed by mafic dykes and then felsic dykes, microgranite and syenite.

A prominent set of vertical fractures are developed in the volcanic complex (Fig. 3a). Previous structural mapping of the area interpreted the trachytic units to be steeply dipping lavas close to vertical (Stephens & Devey 1992), each lava flow bound by bedding surfaces. We observed, however, that the alignment of 'bedding planes' follows the structural alignment in the intruding microsyenites. We therefore favour a structural interpretation where the trachytes are bound by fracture planes and not bedding planes (Fig. 3a, b), as no primary structures or other lines of evidence for steep bedding surfaces can be put forward. This implies that the trachytes are structurally bound eruptive units.

Previous dating

The chron 27r age for the oldest oceanic crust NE of Seychelles inferred from magnetic anomaly data was extrapolated to the identified continental–ocean boundary, interpreted from magnetic, gravity and refraction data, and was used to date the age of break-up between Seychelles and Laxmi Ridge/Indian plate as 63.4 Ma (Collier *et al.* 2008). This age correspond to chron C28n (GST2004) and is roughly similar to ages previous obtained from the alkaline igneous complexes of Silhouette and North Island on the continental plateau of Seychelles (Dickin *et al.* 1986). We summarize here some of the results of Dickin *et al.* (1986). A Rb/Sr whole rock isochron was defined by rocks from Silhouette at 63.2 ± 1 Ma (no. 1 in Fig. 4; all ages reported with 2σ errors), while rocks from North Island yielded only an errorchron. A combined regression of Silhouette and North Island samples gave 63 ± 2.2 Ma. The K/Ar analyses from Silhouette indicated a weighted mean age of 63.7 ± 1 Ma (no. 2 in Fig. 4) for the syenite, 62.1 ± 1.3 Ma (no. 3 in Fig. 4) for the trachyte tuffs and a weighted mean age of 60.23 ± 1.1 Ma (no. 4 in Fig. 4) for the granitic suite. The K/Ar ages obtained from North Island ranged from 65 to 62 Ma, but the authors found the feldspar dates less reliable. A weighted mean age for the ferromagnesian minerals gave 63.3 ± 0.9 (no. 5 in Fig. 4). The dates of Dickin *et al.* (1986) have large uncertainties however, too large to tie the formation of these volcanic complexes to a specific magnetochron in the geomagnetic polarity timescale at an acceptable level of probability. An unpublished, combined U–Pb zircon date of 63.3 ± 0.2 Ma is mentioned in Tucker *et al.* (2001) for syenitic units in Silhouette Island.

Sampling

Samples for palaeomagnetic analysis were taken from the island of Silhouette at locations from Pointe Ramasse Tout to Pointe Vareur (Fig. 2) where fresh outcrops of trachytic tuffs and syenitic

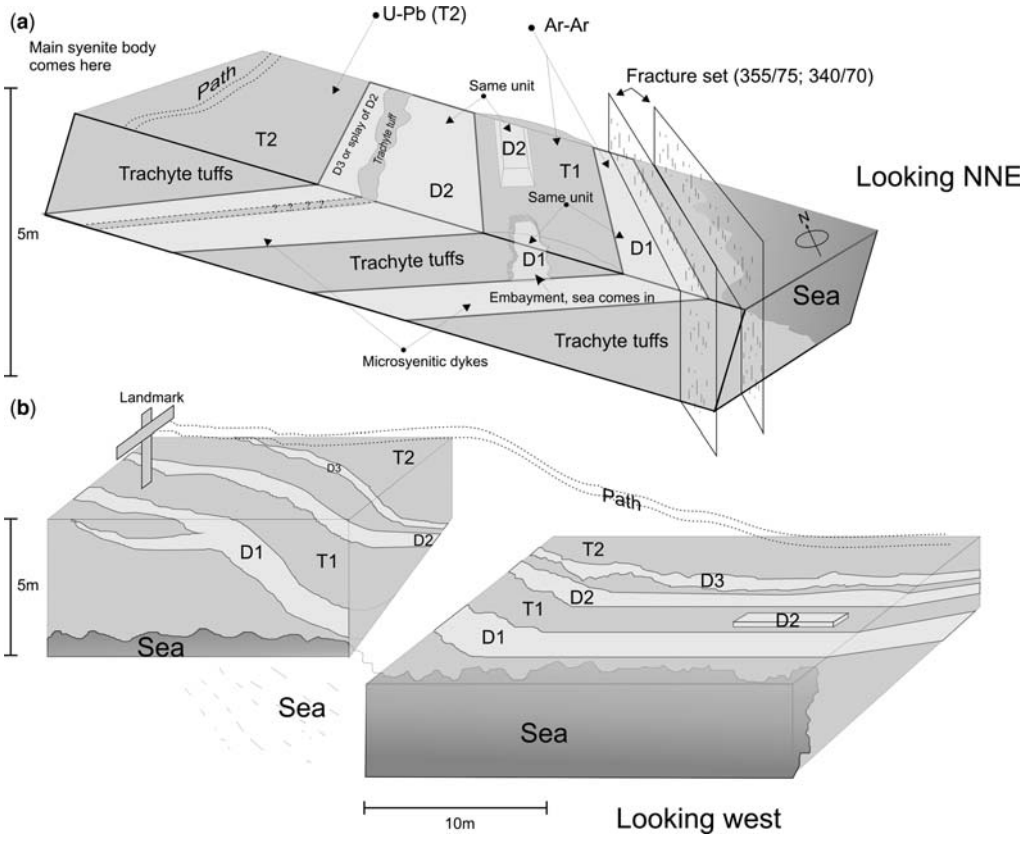

Fig. 3. Structural interpretation of sampling site A looking towards the (**a**) north and (**b**) west. The syenitic dykes (sheeted dykes) becomes more vertical towards the cross (a landmark). Units D1–3 (syenitic dykes) and T1–2 (trachyte tuffs) are the palaeomagnetic sampling sites (see Table 3). The microgranites are not indicated but occur as small patches, one at the cross (Site A). The apparent tilt of the sheeted dykes is less than indicated in the figures.

dykes are exposed. Deccan feeder dykes have also been documented on Prasilin Island (Devey & Stephens 1991), but we had limited time to include those in this study. We have divided the palaeomagnetic sampling locations into sites A to D (Fig. 2). The main syenite body was too coarse-grained to be suitable for palaeomagnetic analysis. A total of 96 25 mm drill cores were extracted from 15 sites with a portable gasoline drill. The orientations of the cores were determined with both magnetic and sun compasses. Due to a very strong local magnetic anomaly (magnetic deviation commonly exceeded 60°), only orientations based on sun azimuth were used. In addition, we sampled the main units (main syenite body, trachyte tuff, microsyenitic sheeted dykes and microgranite) from site A on Silhouette (Figs 2 & 3a, b) for age determination, together with selected sites from North Island (Fig. 2).

$^{40}Ar/^{39}Ar$ age determinations

Samples were crushed and sieved to isolate grains of 180–250 μm. Magnetic separation using a Frantz isodynamic separator, followed by heavy liquid separation with lithium polytungstate, was then employed to concentrate feldspars. Biotite and amphiboles were handpicked after magnetic separation. The mineral separates were washed in acetone several times and finally fresh inclusion-free minerals grains were handpicked under the binocular microscope. Mineral samples were packed in aluminium capsules together with the Taylor Creek rhyolite (TC) flux monitor standard (between each fifth sample, every *c.* 8 mm) and zero-aged K_2SO_4 and CaF_2 salts. The transformation $^{39}K(n, p)^{39}Ar$ was performed during irradiation at the McMaster nuclear facility, Hamilton, Canada. The samples were step-heated in the

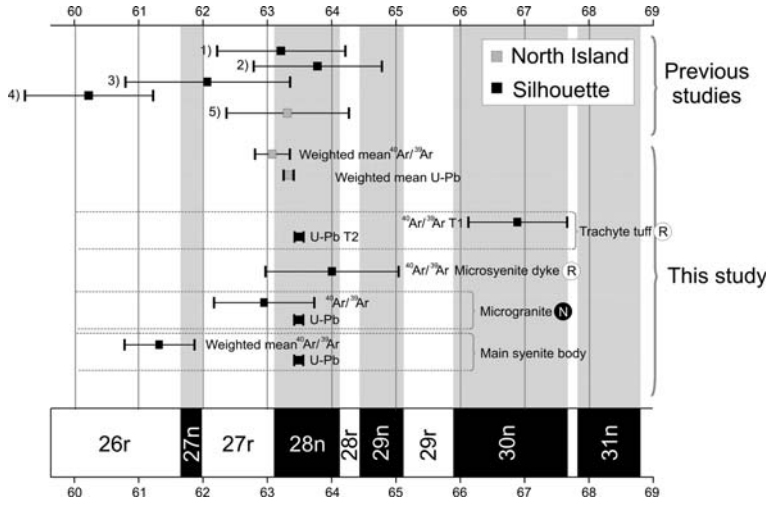

Fig. 4. Dates from North and Silhouette Island with the geomagnetic polarity timescale. Samples labelled 'Previous studies' are from Dickin *et al.* (1986) and are labelled from 1–5 according to the text. Timescale is from Ogg & Smith (2004). The error bars are plotted at the 95% confidence level. The black (N) and white (R) circles are the magnetic polarities found from the palaeomagnetic investigation. The weighted mean ages for North Island are calculated from samples NI1, NI28 and NI32 ($^{40}Ar/^{39}Ar$) and NI-1, NI-2, NI-3 and NI-4 ($^{206}Pb/^{238}U$). The weighted mean age for the main syenite body from Silhouette is calculated from samples Syenite 2 and Syenite 3 ($^{40}Ar/^{39}Ar$). See Table 1 for age summary.

$^{40}Ar/^{39}Ar$ lab at the Geological Survey of Norway using a resistance furnace (Heine type). The extracted gases were swiped over getters (SAES AP-10) for 2 min, and then for 9 min in a separate part of the extraction line. The gas was finally analysed with a MAP 215–50 mass spectrometer. The peaks were determined by peak hopping (at least 8 cycles) on masses ^{41}Ar to ^{35}Ar on a Balzers electron multiplier.

Subtraction of blanks, correction for mass fractionation, correction for $^{37,39}Ar$ decay and neutron-induced interference reactions produced in the reactor were carried out using in-house software (Age Monster 2010, written by M. Ganerød) which implements the equations in McDougall & Harrison (1999) using the decay constants and the trapped $^{40}Ar/^{36}A$ ratio of 295.5 $\pm$ 0.5 of Steiger & Jäger (1977). The decay constants and the correction factors for the production of isotopes from Ca and K can be found in the Supplementary Material. Uncertainties from the blanks, mass discrimination value, salts, trapped constants and every mass balance calculation are propagated into the final age uncertainty. The blanks were measured at temperatures of 450, 700, 1000, 1130 and 1280 °C. The blanks and associated errors for the respective temperature steps for the unknowns were determined using linear interpolation. We used the age of 28.34 $\pm$ 0.16 Ma for the TC monitor (Renne *et al.* 1998) during data reduction. We define a plateau according to the following requirements: at least three consecutive steps each within 95% confidence level:

$$\text{abs}(\text{age}_A - \text{age}_B) < 1.96 \times \sqrt{\sigma_A^2 + \sigma_B^2}$$

if ages are quoted at the 1σ level

comprising at least 50% of total ^{39}Ar and mean square of weighted deviates (MSWD) less than the student *T* critical value. We calculated a weighted mean plateau age (WMPA), weighting by the inverse of the variance.

The step-heating spectra with plateaus are depicted in Figure 5 and the main results from spectrum and inverse isochrons analysis are displayed in Table 1 (the raw experimental data are located in the Supplementary Material). Figure 5 shows that most samples have a slight Ar loss, most likely due to the presence of small amounts of alteration in all age spectra at the lowermost temperature steps, but concordant plateaus are obtained in all analyses. The K/Ca ratios show some variation, which we relate to compositional differences and/or inclusions. However, the variation does not seem to affect the apparent ages. The mean square of weighted deviates (MSWD) indicates a generally good correspondence between expected and estimated errors. Some of the apparent ages from the different units on Silhouette are different at the 95% confidence level so we treat them here as separate cooling ages.

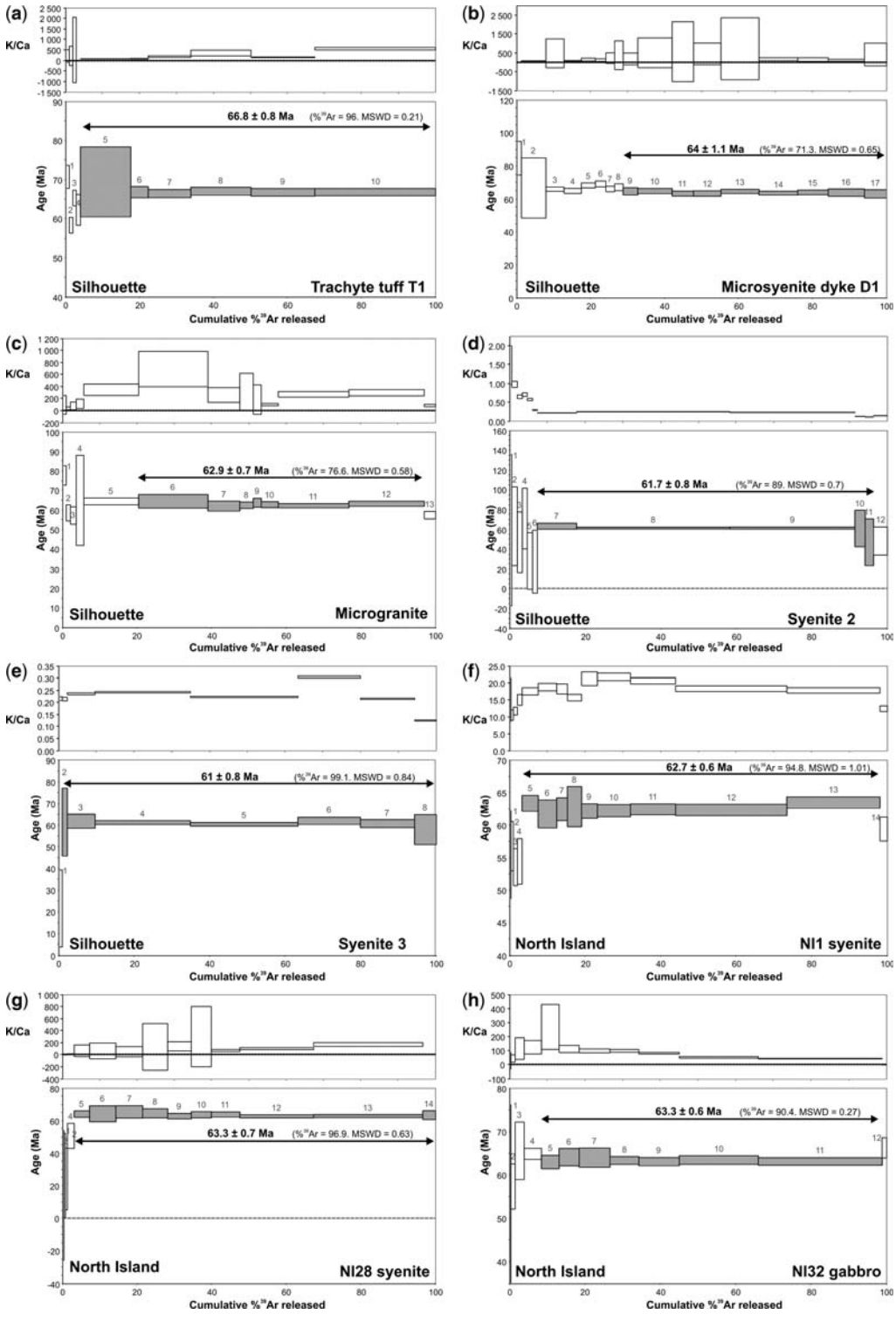

Fig. 5. Step heating release spectra for the samples from Silhouette and North Island. Each age bar is plotted at 95% confidence level. The numbers above the age bars correspond to the row number in the Supplementary Material.

Table 1. *Main results from step heating analysis*

Location	Rock type	Spectrum analysis				MSWD	TFA	K/Ca $\pm 1.96\sigma$	Inverse isochron analysis		
		^{39}Ar %	Steps (N)	Age (Ma)	$\pm 1.96\sigma$				Age (Ma) $\pm 1.96\sigma$	MSWD	Intercept $\pm 1.96\sigma$
North Island	NI1 syenite^{K}	94.77	5–13 (9)	62.65	0.36/**0.55**/0.55	1.01	62.37 ± 0.57	18.77 ± 0.7	62.71 ± 0.63	1.15	293.68 ± 12.49
	NI28 syenite^{B}	96.91	5–14 (10)	63.34	0.50/**0.65**/0.65	0.63	62.82 ± 0.78	11.85 ± 2.2	62.79 ± 0.85	0.26	315.48 ± 21.31
	NI32 gabbro^{K}	90.39	5–11 (7)	63.34	0.42/**0.59**/0.59	0.27	63.47 ± 0.63	53.73 ± 3.5	63.27 ± 0.7	0.31	299.12 ± 19.47
Silhouette	Trachyte tuff^{K}	96.02	5–10 (6)	66.84	0.46/**0.75**/0.76	0.21	67.10 ± 1.41	116.14 ± 12.7	66.75 ± 0.82	0.21	299.28 ± 15.37
	Microsyenite dyke^{K}	71.25	9–17 (9)	64.00	0.52/**1.09**/1.10	0.65	65.02 ± 1.62	147.41 ± 78.4	64.08 ± 1.25	0.74	293.02 ± 19.97
	Microgranite^{A}	76.58	6–12 (7)	62.91	0.61/**0.73**/0.74	0.58	63.33 ± 1.02	147.65 ± 31.1	62.81 ± 1.12	0.69	297.24 ± 15.08
	Syenite 2^{B}	89.04	7–11 (5)	61.67	0.64/**0.81**/0.81	0.70	60.03 ± 1.57	0.18 ± 0.003	61.91 ± 1.27	0.87	292.86 ± 11.2
	Syenite 3^{B}	99.08	2–8 (7)	61.01	0.53/**0.80**/0.80	0.84	60.63 ± 0.94	0.20 ± 0.002	60.91 ± 0.96	0.99	296.98 ± 8.05

The plateau age uncertainties are reported as analytical/internal/external errors where internal includes analytical + experimental error on the J and the fluence age uncertainties; external error includes internal error + the uncertainties on the decay constant. TFA, total fusion age (K/Ar age). The superscript in the Rock type column denotes the mineral used in analysis (K, potassium feldspar; B, biotite; A, amphibole).

The Silhouette samples yield a wide spread of ages (Fig. 5a–e) from 66.8 ± 0.8 Ma (trachyte tuff) to 61 ± 0.8 Ma (main syenite body). The microsyenite dyke (D1) and the microgranite yield 64 ± 1.1 Ma and 62.9 ± 0.7 Ma, respectively. The two samples from the main syenite body in Silhouette (Fig. 5d, e; Table 1) and the three samples from North Island (Fig. 5f–h; Table 1) overlap at the 95% level and we calculate weighted mean ages which give 61.3 ± 0.57 and 63.1 ± 0.34 Ma, respectively. These results are considered in the Discussion (p. 242).

U/Pb age determinations

Zircon was extracted from four samples from North Island and three from Silhouette by using a sequence of jaw crusher, pulverizing mill, Wilfley table, sieving, magnetic separation and heavy liquid methylene iodide (MI) floatation. Suitable grains were selected for analyses by hand-picking under a binocular microscope. The coherent results reported here were obtained by treating the zircon with mechanical abrasion (Krogh 1982) whereas (except for sample microgranite) chemical abrasion (Mattinson 2005) provided only variably discordant data (Corfu 2009). The analyses were carried out by ID-TIMS following Krogh (1973) as described for the Oslo laboratory in Corfu (2004). Decay constants are those of Jaffey *et al.* (1971) and plotting was carried out using the program of Ludwig (2003).

All the analyses yield overlapping $^{206}Pb/^{238}U$, but all the more precise results plot to the right of the concordia curve (Table 2 & Fig. 6). This discrepancy between $^{206}Pb/^{238}U$ and $^{207}Pb/^{206}Pb$ is confirmed by the precise analyses of the chemical abrasion experiments (Corfu 2009), which will be presented and discussed in detail in a subsequent paper. The deviation towards higher $^{207}Pb/^{206}Pb$ ages cannot be explained by the decay constant bias (Schoene *et al.* 2006) nor by isotopic disequilibrium, as all the data are corrected for ^{230}Th deficit assuming a Th/U of 4 in the parent magma (the correction increases $^{206}Pb/^{238}U$ by about 0.1 Ma).

The most important observation is the reproducibility of the $^{206}Pb/^{238}U$ ages, which give weighted average values ranging from 63.20 ± 0.12 to 63.31 ± 0.11 Ma for the North Island samples and from 63.46 ± 0.14 to 63.58 ± 0.09 Ma for the Silhouette samples (Fig. 6). Weighted averages for all the samples from North Island and Silhouette gives 63.27 ± 0.05 and 63.54 ± 0.06 Ma, respectively. The consistent results indicate very rapid emplacement of the complexes but with a time gap, with magmatism on Silhouette preceding the events on North Island by 0.27 ± 0.08 Ma.

Palaeomagnetic analysis

Palaeomagnetic laboratory experiments were carried out at the Geological Survey of Norway (Trondheim, Norway). The natural remanent magnetization (NRM) was measured on an AGICO JR6A spinner magnetometer mounted within a Helmholtz coil system. Components of magnetization were identified using stepwise thermal and alternating field demagnetization. All specimens were demagnetized in 15–25 steps. The directions and unblocking temperature spectra of characteristic remanence components (ChRM) were determined using the LineFind algorithm of Kent *et al.* (1983) as implemented in the Super-IAPD program available at www.geodynamics.no (Torsvik *et al.* 2000). For those specimens where the ChRM could not be isolated directly where they defined a circle of remagnetization (Khramov 1958), we used the plane fits output from the LineFind algorithm and the great circle principle of McFadden & McElhinny (1988) implemented in the Palaeomag–Tools software (written by Mark W. Hounslow). In the Palaeomag–Tools software we set a fixed point (to force the polarity), but the point is not included in the statistics.

A set of rock magnetic experiments was performed to reveal the magnetic mineral host, using a horizontal Curie Balance for thermomagnetic measurements and a vibrating sample magnetometer (VSM) to produce hysteresis loops. The thermomagnetic investigation (Fig. 7a) on selected samples from all units reveals Curie temperatures close to those of pure magnetite (580 °C). This is supported by the VSM experiments (Fig. 7b), which are indicative of a ferromagnetic mineral phase with low coercivity. Further M_{rs}/M_s against H_{cr}/H_c (Day *et al.* 1977) shows that the magnetizations are carried by pseudo-single domain and a mixture of pseudo and multidomain grains for all units (Fig. 7c). We therefore conclude that the magnetic mineral host is dominantly magnetite or Ti-poor titanomagnetite.

The site mean directions, estimators, NRM intensities, magnetic susceptibilities and Q-ratios (Königberger) can be found in Table 3. The results from thermal demagnetization were unsuccessful for all sites apart from one because they display a within-site randomness of ChRM directions. Even closely spaced cores showed this behaviour, although most specimens show univectorial demagnetization behaviour towards the origin (Fig. 8a). This behaviour is often seen in rocks that experienced an isothermal remanent magnetization (IRM) caused by lightning strike (Hallimond & Herroun 1933).

Specimens commonly have very high NRM intensities in the range of 5–20 A/m, supporting the inferred influence of lightning strikes.

Table 2. *Zircon U–Pb data*

Characteristics[1]	Weight[2,3] (μg)	U[2,3] (ppm)	Th/U[4]	Pbc[3] (pg)	$^{206}Pb/^{204}Pb$[5]	$^{207}Pb/^{235}U$[5]	$\pm 2\sigma$ (abs)	$^{206}Pb/^{238}U$[6,7]	$\pm 2\sigma$ (abs)	rho	$^{207}Pb/^{206}Pb$[6,7]	$\pm 2\sigma$ (abs)	$^{206}Pb/^{238}U$[6,7] (age in Ma)	$\pm 2\sigma$	$^{207}Pb/^{235}U$[6,7]	$\pm 2\sigma$
NI-1 syenite, North Island																
fr [1]	46	360	1.04	1.4	7130	0.06433	0.00018	0.00984	0.00002	0.81	0.04740	0.00008	63.20	0.20	63.31	0.20
fr cl [10]	173	746	0.94	1.3	59 764	0.06457	0.00018	0.00987	0.00003	0.97	0.04744	0.00003	63.38	0.20	63.53	0.20
fr cl [3]	97	607	1.04	2.9	12 340	0.06436	0.00017	0.00986	0.00002	0.94	0.04736	0.00004	63.28	0.10	63.34	0.20
NI-2 syenite, North Island																
fr cl [22]	254	866	1.46	4.6	29 315	0.06425	0.00019	0.00983	0.00003	0.97	0.04739	0.00003	63.13	0.17	63.23	0.18
fr y-b [1]	210	517	1.11	7.9	8470	0.06456	0.00018	0.00988	0.00002	0.95	0.04738	0.00004	63.45	0.15	63.53	0.17
NI-3 microsyenite, North Island																
fr cl [37]	45	859	2.04	3.2	7458	0.06429	0.00018	0.00984	0.00002	0.89	0.04739	0.00006	63.17	0.15	63.27	0.17
fr cl-y [12]	49	242	1.36	3.0	2476	0.06430	0.00024	0.00985	0.00003	0.69	0.04735	0.00013	63.22	0.18	63.27	0.23
NI-4 gabbro, North Island																
fr cl [9]	56	1909	2.31	5.0	13 163	0.06448	0.00018	0.00985	0.00003	0.96	0.04747	0.00004	63.24	0.20	63.45	0.20
fr cl [2]	48	1708	1.89	1.3	38 780	0.06450	0.00018	0.00985	0.00003	0.96	0.04748	0.00004	63.25	0.20	63.46	0.20
SI-1 syenite, Silhouette																
fr-eu cl [30]	34	544	1.42	6.6	1757	0.06461	0.00022	0.00990	0.00002	0.72	0.04733	0.00011	63.56	0.20	63.57	0.20
fr-eu cl [33]	63	510	1.56	4.9	4047	0.06480	0.00019	0.00990	0.00003	0.85	0.04750	0.00007	63.53	0.16	63.75	0.18
T2 trachyte, Silhouette																
fr-eu cl [18]	12	616	1.50	1.6	2902	0.06448	0.00030	0.00989	0.00003	0.71	0.04731	0.00015	63.47	0.20	63.45	0.28
fr-eu cl in [17]	8	423	1.43	4.3	507	0.06481	0.00062	0.00988	0.00003	0.48	0.04755	0.00040	63.46	0.20	63.76	0.59
Microgranite, Silhouette																
eu sp cl-tu CA [20]	60	289	0.93	2.3	4649	0.06474	0.00024	0.00990	0.00003	0.73	0.04744	0.00012	63.54	0.19	63.70	0.22
eu sp cl CA [25]	47	363	1.05	2.1	5073	0.06473	0.00019	0.00991	0.00002	0.78	0.04736	0.00009	63.64	0.15	63.69	0.18
eu sp cl [11]	17	580	1.16	12.9	493	0.06439	0.00051	0.00990	0.00003	0.36	0.04718	0.00035	63.55	0.16	63.37	0.49

[1]fr, fragments; eu, euhedral; sp, short prismatic (l/w = <4); cl, clear, colourless; r, red; y, yellow; b, brown; tu, turbid spots; incl, in; CA, chemically abraded (Mattinson 2005), all the others mechanically abraded (Krogh 1982); [N], number of grains in fraction.
[2,3]Weight and concentrations are known to better than 10%.
[4]Th/U model ratio inferred from 208/206 ratio and age of sample.
[3]Pbc = total common Pb in sample (initial + blank).
[5]Raw data corrected for fractionation and blank.
[6]Corrected for fractionation, spike, blank and initial common Pb; error calculated by propagating the main sources of uncertainty.
[7]Corrected for initial Th deficit assuming Th/U in the magma = 4 (Schärer 1984).

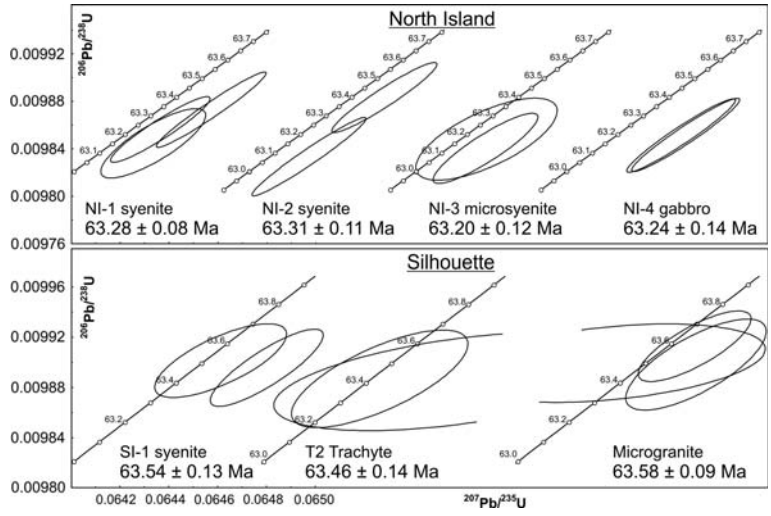

Fig. 6. Composite concordia diagrams with U–Pb data for zircon in samples from the two islands. Ellipses indicate the 2σ uncertainty of the analyses, which are also corrected for initial Th deficit. The ages represent weighted mean $^{206}Pb/^{238}U$ dates for each sample.

Alternating-frequency (AF) demagnetization proved more successful in determining the ChRM from the lightning-induced component. Figure 8a, b shows the difference between thermal and AF demagnetization applied to samples from the same core. The two components partly overlap in most samples, spanning remagnetization great circles. Because the lightning-induced remagnetization direction varies from sample to sample, the common intersection point of all great circles can be identified and is interpreted as the ChRM (Fig. 8c, d). For most sites the demagnetization curve does not reach a stable endpoint (i.e. Fig. 8c). Figure 8d however shows an example

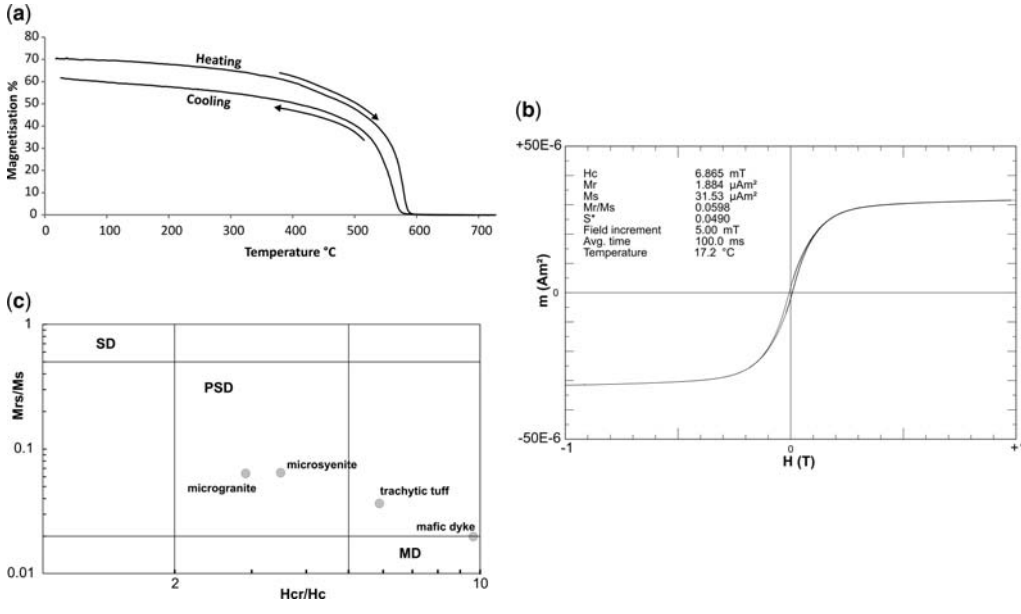

Fig. 7. Rock magnetic experiments: (**a**) Curie-temperature, (**b**) hysteresis and (**c**) Day plot where SD, PSD and MD denote single, pseudo-single and multi-domains, respectively.

Table 3. *Palaeomagnetic sampling sites and results*

Site	Unit	Comment	D	I	N	R	k	A95	NRM_{int}	Sus	Q	VGPLat	VGPLong	Dp	Dm
A	MS D1*	Dyke	146.9	6.2	10	9.97	186.7	4	36 718	33 882	27.2	−56.9	146.5	2	4
	T1*	Flow	153.1	47.5	5	4.99	288.68	9.3	60 626	42 058	36.2	−54.9	98.9	7.9	12.1
	T1*	Flow	178.9	45.1	6	5.94	48.13	10.8	42 689	59 761	18	−67.8	57.9	8.7	13.7
	T1*	Flow	142.7	9.7	4	3.98	171.87	7	23 254	32 827	17.8	−52.8	143.1	3.6	7.1
	MS D2*	Dyke	152.6	13.3	5	5.97	80.26	9.8	61 377	30 393	50.8	−62.6	139.3	5.1	10
	MS D3*	Dyke	163	18.5	6	5.99	638.86	2.7	15 284	18 770	20.5	−72.4	127.8	1.5	2.8
	T2*	Flow	140.2	28.4	3	2.99	58.5	8.1	44 539	59 549	18.8	−49.4	127.1	4.9	8.9
	T2*	Flow	124.7	56	4	4	328.97	9.8	13 338	25 400	13.2	−30.2	105.1	10.1	14.1
	Microgranite*	At cross	319.8	−63.8	9	8.97	104.83	6	43 552	25 093	43.6	−36.1	89.4	7.6	9.5
B	Microgranite*		296.3	−28.1	8	7.91	32.24	11.2	38 293	18 821	51.1	−26.5	130.8	6.7	12.3
	Flow*		166.5	11.4	8	7.93	45.66	9.7	159	2071	1.9	−76.5	139.3	5	9.8
C	Mafic dyke*		129.9	27.1	7	6.94	44.28	12.2	6099	57 921	2.6	−39.7	130.3	7.2	13.3
	Dyke*		172.4	16.7	4	3.99	563.67	7.4	789	20 055	1	−81.4	116.7	3.9	7.6
D	Trachyte tuff		131.4	32.1	4	3.98	26.2	26.2	5999	50 786	3	−40.7	126.1	16.6	29.5
	Dyke*		188.6	64.5	5	5	895.2	5.3	1224	22 316	1.4	−47.5	46.5	6.8	8.5
			D	ΔD_x	I	ΔI_x	N					PLat	Plong	K	A95
	Mean		150.6	12.9	32.4	19.3	14					−57.55	114.22	11.4	12.3

D/I, declination/inclination of flow mean remanence directions; N, number of remanence directions; R, length of resultant vector; k and A95 are the Fisher (1953) precision parameter and half angle of the cone of 95% confidence. NRM_{int} denotes moment intensities (mA) and Sus are the susceptibilities (10−5 SI) before heating. Q is the Königsberger ratio based on an ambient field strength of 50 000 nT which is 39.79 A m^{-1}. Units marked with an asterisk (*) are used in the calculation of the overall mean direction and the pole.

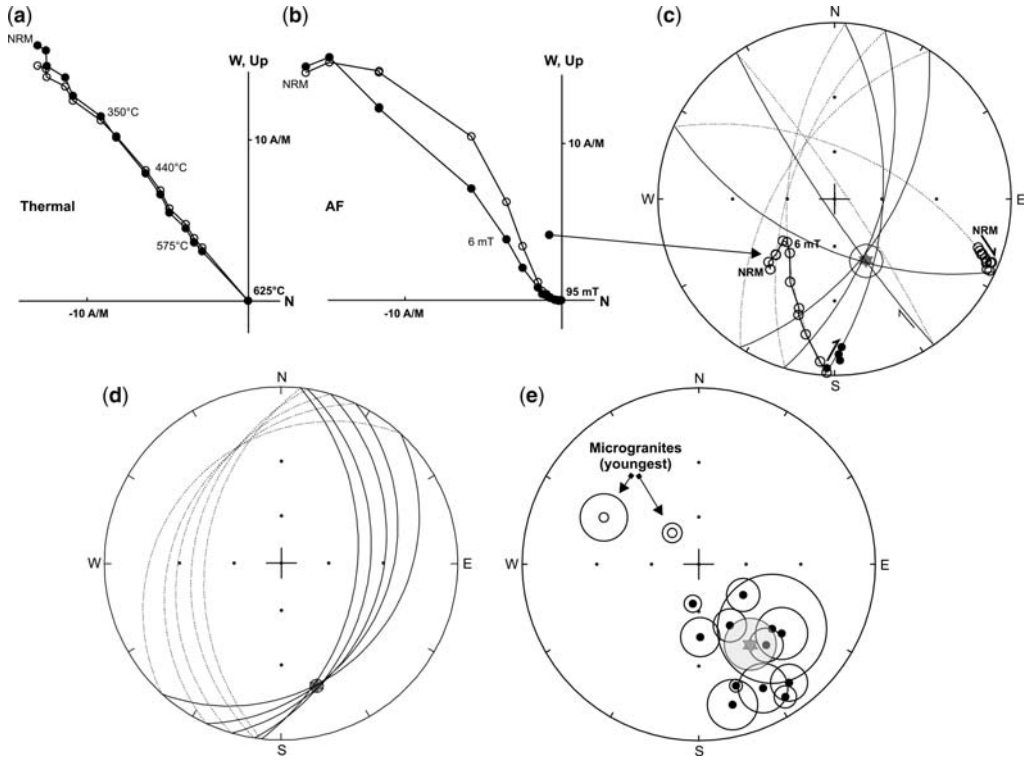

Fig. 8. Stepwise thermal and AF demagnetization data visualized in orthogonal and stereographic plots. For the orthogonal plots solid (open) symbols represent data projected into the horizontal (vertical) plane and for the stereoplots equal area projections are used where black (white) circles represent reverse (normal) polarities (southern hemisphere). (**a**) Thermal demagnetization produces linear decay towards the origin, (**b**) while AF from a specimen from the same core produces a great circle path. The sample in (b) is displayed in (**c**) together with several samples from the same site defining a common intersection point but no stable endpoint (b). (**d**) Shows an example where a stable endpoint was reached and also produces the same direction using great circle analysis. All site mean directions are plotted in (**e**) with A95 confidence circles. The overall mean direction is represented by a grey star.

where a stable endpoint was reached, leading to a direction statistically indistinguishable from one derived through great circle analysis.

We interpret all the characteristic component directions obtained from the 15 sites as a reliable record of the Earth's magnetic field at their time of emplacement. The results show that all sites except the microgranites are of reversed polarity (Fig. 8e, Table 3). The microgranites cross-cut the other units, and are therefore the youngest unit in the volcanic complex. Only the syenite is younger, but that was not analysed palaeomagnetically.

Because dispersion within a single lava site should be minimal, a stringent cut-off is normally applied; lava sites with *k*-values lower than 50 (Biggin *et al.* 2008; Johnson *et al.* 2008; van Hinsbergen *et al.* 2008*a*, *b*) are discarded. Of our 15 sites, 5 have a *k*-value below 50. Because of the relatively small dataset, we include 4 sites with *k*-values between 30 and 50 (Table 3) in our average to increase our statistical power; this does not lead to a significantly different average direction. Averages and cones of confidence were determined using Fisher (1953) statistics applied to Virtual Geomagnetic Poles (VGP), because these are more Fisherian (i.e. a Gaussian dispersion on a sphere) than directions which have a (latitude-dependent) elongated distribution (Tauxe & Kent 2004; Tauxe *et al.* 2008; Deenen *et al.* 2011). Errors in declination and inclination are given separately as ΔD_x and ΔI_x (Butler 1992; Deenen *et al.* in revision) in Table 3. No directions were eliminated by the Vandamme (1994) variable cut-off procedure. We therefore arrive at a $D \pm \Delta D_x = 150.6 \pm 12.9$ and $I \pm \Delta I_x = 32.4 \pm 19.3$ ($n = 14$).

The degree of palaeosecular variation can be expressed through the angular standard deviation (ASD) of the virtual geomagnetic poles (VGP) if

the VGPs have a Fisherian distribution. To test whether this is true, we performed a quantile–quantile calculation (Fisher *et al.* 1987). The goodness of fit to the Fisherian distribution for the VGPs is lower than the critical values ($Mu = 0.803 < 1.207$, $Me = 0.509 < 1.094$) and the null hypothesis that the distribution of VGPs is Fisherian cannot be rejected at the 95% confidence level (Fisher *et al.* 1987). The ASD of VGPs, corrected for within-flow dispersion $Sw = 5.3^\circ$ (McFadden *et al.* 1991), is 12° with a 95% confidence limit of $9.6 \leq ASD \leq 16$ (Cox 1969). This ASD is within error of the PSV prediction of the G-model of McFadden *et al.* (1991), which indicates an ASD value of *c.* 11 for this time and palaeolatitude. We therefore conclude that the observed dispersion can be explained by secular variation and the determination of the overall mean direction satisfactorily represents the palaeosecular variation.

Ideally, remanence directions should be Fisherian distributed close to the poles but ellipsoid elsewhere (Tauxe & Kent 2004). To determine a palaeomagnetic pole for this study, we therefore apply Fisher (1953) statistics on the VGPs which leads to an apparent palaeomagnetic pole position at 57.55°S and 114.22°E ($k = 11.4$; $A95 = 12.3$; Table 3) in Seychelles co-ordinates.

Discussion

Timing of emplacement

The new $^{40}Ar/^{39}Ar$ and U–Pb determinations and 95% confidence bars from North and Silhouette islands are displayed in Figure 4, together with the geomagnetic polarity time scale (Ogg & Smith 2004). The chron boundaries are intercalibrated with an age of 28.34 Ma for the TCR fluence monitor used here to derive the $^{40}Ar/^{39}Ar$ data. The accuracy of the U–Pb ages is dependent largely on the spike calibration; measurements of reference solutions indicate that our spike is within about 1 permil of accepted values, translating into a potential bias of less than 0.07 Ma for this age range.

The $^{40}Ar/^{39}Ar$ dates obtained from K-feldspar in gabbro and syenite N1 and from biotite in syenite NI28 on the North Island are identical within error and yield a weighted mean age of 63.1 ± 0.34 Ma, which overlaps the U–Pb weighted mean of 63.27 ± 0.05 Ma and corresponds to chron C28n (Fig. 4). This also resembles previous age determinations from the North Island (Dickin *et al.* 1986; Tucker *et al.* 2001) and the 63.4 Ma age assigned to the oldest ocean floor anomaly between the Seychelles and the Laxmi ridge by Collier *et al.* (2008).

The $^{40}Ar/^{39}Ar$ dates obtained from the Island of Silhouette range from 66.8 ± 0.8 Ma for K-feldspar in trachyte tuff T1, over 64 ± 1.1 Ma for K-feldspar in microsyenite D1 and 62.9 ± 0.7 Ma for hornblende in microgranite, to 61.7 ± 0.8 and 61 ± 0.8 Ma for biotite in syenites 2 and 3 (Fig. 4). The age of 66.8 ± 0.8 Ma for the trachytic unit contrasts with zircon U–Pb age for a similar tuff at 63.46 ± 0.14 Ma. The latter is slightly younger but within error of the U–Pb ages of 63.58 and 63.54 Ma for syenite and microgranite (Figs 4 & 5). Even though the sample for U–Pb analysis comes from a separate trachyte unit located higher in the sequence (see Fig. 3), all the tuffs share the same macroscopic texture and characteristics and hence the age difference is difficult to explain. Dickin *et al*. (1986) suggested that their 62.1 ± 1.3 Ma age from this unit should be regarded as a minimum age due to the tendency of acid whole-rock samples to lose argon.

Our total fusion age of the K-feldspar in the trachyte (TFA, Table 1) does not resemble the results of Dickin *et al.* (1986) either. We obtained a plateau comprising 96% of the total ^{39}Ar released and the date resembles the inverse isochron and the TFA. In search of any potential systematic errors, we note that the J parameter determination for this sample is also in the range of the other samples. We notice that the trachyte contains xenoliths of a rock type of unknown age with syenitic composition (Owen-Smith *et al.* pers. comm.); one possibility is that the K-feldspar is xenocrystic and was picked up during eruption, thus escaping outgassing. This possibility will have to be tested by additional dating on the trachyte and xenoliths. Until then, we are reluctant to put too much weight on this age which would put volcanism during chron C30n (Fig. 8) at the onset of the main Deccan tholeiitic eruptions. Early acidic and alkaline volcanism is known from the north of the Deccan Province, but trachytic eruptions of this type are more commonly associated with the late-stage volcanics at 60–63 Ma (chron C28n and later).

The $^{40}Ar/^{39}Ar$ ages for K-feldspar in the microsyenite (64 ± 1.1 Ma) and amphibole in the microgranite (62.9 ± 0.7 Ma) overlap the zircon U–Pb ages. By contrast, the weighted mean $^{40}Ar/^{39}Ar$ age of 61.3 ± 0.6 Ma for the biotite in syenites of Silhouette are younger than the U–Pb zircon age 63.54 ± 0.13 Ma and previous age determinations, including the 63.7 ± 1 Ma whole-rock K/Ar age of Dickin *et al.* (1986). Biotite has a relatively low closing temperature for Ar and the age may reflect slow cooling of the area. The alternative is that the older zircon U–Pb age represents pre-emplacement formation in the magma chamber (Crowley *et al.* 2006; Miller *et al.* 2007), although the overlap with the amphibole and K-feldspar $^{40}Ar/^{39}Ar$ ages

and the coherence between these systems on the North island would seem to argue against this possibility. Moreover, the generally high solubility of Zr in alkalic magmas tends to lead to late precipitation of zircon, a factor militating against protracted residence times of zircon in such magmatic systems.

The magnetic polarities observed in all samples are reverse, except for the microgranite which is normal (Table 3). These relationships represent a mismatch with the timescale used in Figure 4, where all the U–Pb dates and part of the $^{40}Ar/^{39}Ar$ age determinations plot inside C28n; it would fit the Silhouette biotite ages, however. In the simple case of a short-lived volcanic complex undergoing rapid cooling, the magnetic polarities and the ages should coincide with the timescale. The mismatch between the radiometric age determinations and the remanence directions can be interpreted in terms of closure temperature and blocking temperature for magnetic remanence. The thermomagnetic investigation (Fig. 7a) reveals a magnetic carrier with Curie temperatures close to pure magnetite (580 °C). The Curie temperature of magnetite is between the closure temperature of zircon (excess of 900 °C, e.g. Cherniak & Watson 2001) and most minerals used for the $^{40}Ar/^{39}Ar$ system. The palaeomagnetic investigation also reveals that some secular variation has been recorded (e.g. units T1, microgranite and T2 in Table 3). Altogether, this could be interpreted in terms of a slow cooling for the whole complex or that the later main syenite body has generated enough heat for a considerable amount of time to reset the $^{40}Ar/^{39}Ar$ system and distort the magnetic remanence.

Based on the timescale of Ogg & Smith (2004), Collier *et al.* (2008) divided the volcanic record of the region into three stages: pre-Deccan (*c.* 78–67 Ma, 33n–30n), Deccan (*c.* 67–63 Ma, 30n–27r) and post-Deccan (*c.* 63–58 Ma, 27n–26n). Our new U–Pb ages fit chron C28n and overlap with the Deccan stage of Collier *et al.* (2008), which demonstrates that the emplacement of the magmatic rocks of Silhouette was contemporaneous with the Deccan volcanism. An important point to this end is whether these rocks are the product of the same mantle source responsible for the Deccan volcanism. Devey & Stephens (1991) provide a geochemical correlation of dykes from the Seychelles to the Deccan Bushe Formation. A recent study by Owen-Smith *et al.* (pers. comm.) indicates strong geochemical grounds for a common mantle source for the Seychelles and Deccan magmatism. In terms of Sr- and Nd-isotopic compositions in particular, the Silhouette and North island rocks show strong affinities with the uncontaminated magma groups of the Deccan (Ambenali and Mahabaleshwar Formations; see Mitchell & Widdowson (1991) for Deccan chemostratigraphy). This raises the question of how much the areal extent of Deccan Traps can be extended. The Rajahmundry Traps in southeast India have recently been linked to the Deccan (Jay & Widdowson 2008; Self *et al.* 2008) based on geochemical and geochronological evidence (e.g. 64.7 $\pm$ 0.57 Ma from Baksi 2005). The new geochronology presented here, and the geochemical link documented in Devey & Stephens (1991) and Owen-Smith *et al.* (in preparation), certainly extend the Deccan volcanism to the Seychelles.

Regional implications, plate reconstructions and the African Plume Generation Zone

The evolution of the western Indian margin and the formation of oceanic basins between the Madagascar–India/Seychelles, West India/Laxmi Ridge and Seychelles underwent complex tectonic phases that led to several stretched continental crust blocks, volcanic ridges, oceanic basins and possibly incipient subduction zones. Classical studies (Masson 1984) and more recent papers, based on existent and new geological and geophysical data (Bhattacharya *et al.* 1994; Todal & Eldholm 1998; Bernard & Munschy 2000; Lane 2006; Collier *et al.* 2008, 2009; Yatheesh *et al.* 2009), postulate the existence of extended continental crust/sublithospheric mantle and/or oceanic crust in the proximity of the western Indian margin in the Laxmi Basin and the Gop Rift. Originally, Masson (1984) suggested that a fan-shaped region of extended continental crust (or oceanic crust) should be present along the western Indian margin to explain the age and architecture of the Mascarene Basin (between Madagascar and the Seychelles/Mascarene Plateau). The 'missing' crust in the NE could have been created NE of the Seychelles, probably contemporaneous or towards the end of the Mascarene Basin opening. Marine magnetic anomalies have been identified in the Laxmi Basin and the Gop Rift by several authors, although the age of these identifications differs from one study to another. Although we would expect extension and spreading in the Gop Rift (between the Laxmi Ridge and the extended continental crust of west India) to have been extinct at the time of the East Arabian Sea opening (around C28n, 64.1–63.1 Ma on GTS2004 timescale; Ogg & Smith 2004; Lane 2006; Collier *et al.* 2008), a different identification of magnetic anomalies in the Gop Rift (Yatheesh *et al.* 2009) suggest an ongoing activity in this basin for another few million years (C25r, 58.5 Ma on GTS2004) while oceanic crust formed along the Carlsberg Ridge. In addition, the southern

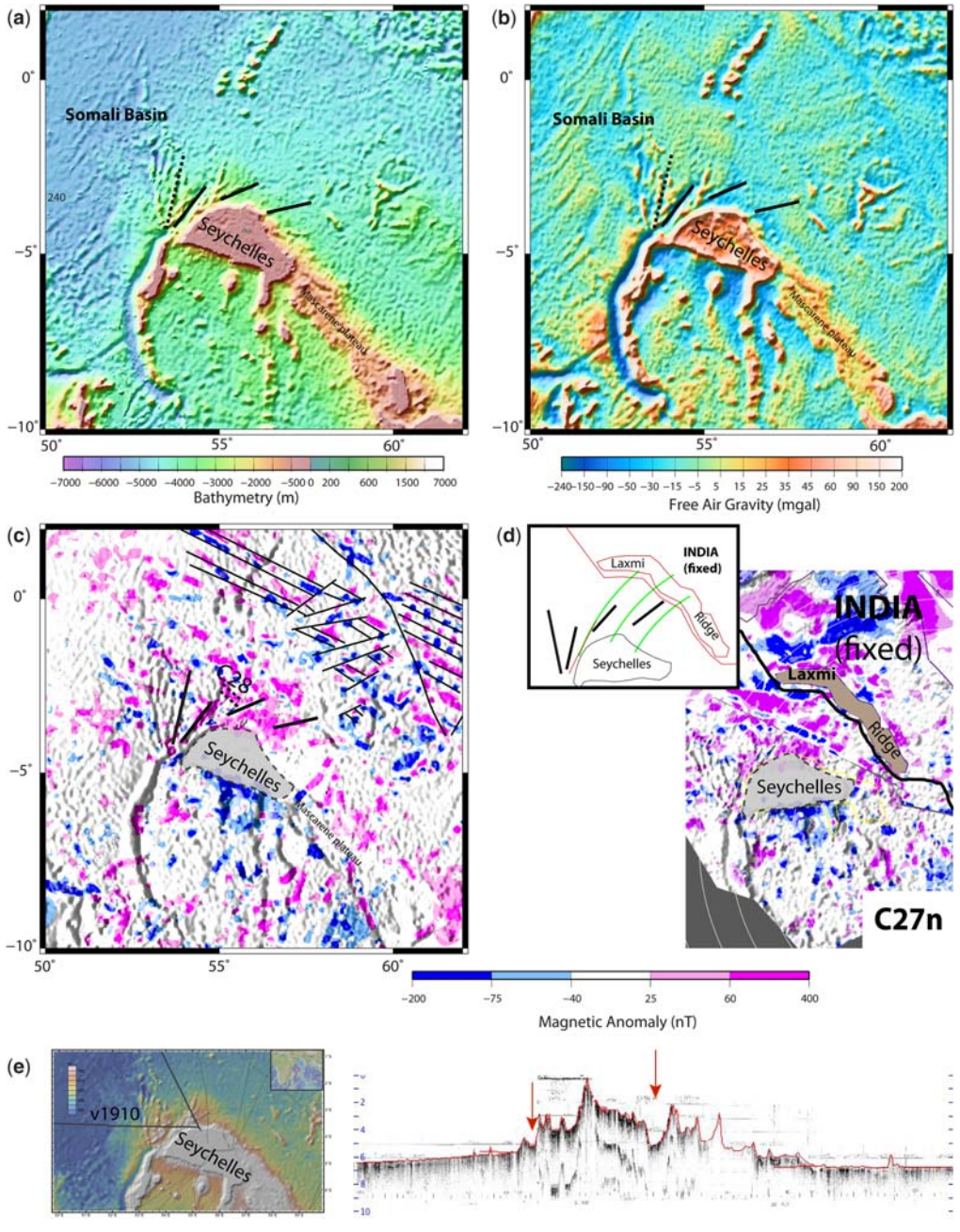

Fig. 9. Seychelles and surrounding areas. The geographical extent of a, b and c are shown in Figure 1. (**a**) Bathymetry (ETOPO1, Amante & Eakins 2009), (**b**) free-air gravity anomaly (Sandwell & Smith 1997) and (**c**) magnetic anomalies from World Digital Magnetic Anomaly Map (Maus *et al.* 2007) superimposed on shaded bathymetry grid (Amante & Eakins 2009). Black, thin lines are isochrons based on magnetic and fracture zone interpretation in the South Arabian Sea (Chaubey *et al.* 2002); dashed, black lines show the approximate location of the oldest chron (C28n) identified by Collier *et al.* (2008); light dashed line represents the outline of the Seychelles microcontinent. Note a fan-shaped set of NNE–SSW to NE–SW features in both bathymetry and free-air gravity (tentatively outlined by thick, black lines) that may indicate an anticlockwise rotation of the Seychelles. (**d**) Reconstructions at chron C27n in a fixed Indian plate reference frame of present-day magnetic anomaly grid (Maus *et al.* 2007) and shaded bathymetry. Reconstructed

extinction of the Mascarene Basin spreading centre occurred *c.* 2 Ma after C27n (Bernard & Munschy 2000), a situation that implies a system of opposed propagating spreading centres in the Mascarene, East Arabian and Gop/Laxmi basins. This scenario has been observed in other regions involving microcontinent formation, for example Jan Mayen in the North Atlantic Ocean (Gaina *et al.* 2009) and the Danakil block in the Red Sea area (e.g. Beyene & Abdelsalam 2005).

Our study shows that the mean palaeomagnetic remanence direction for this part of the Seychelles is translated in an anticlockwise sense of $29.4^\circ \pm 12.9^\circ$. Plummer (1996) pointed out an asymmetry in the spreading rates of the Mascarene Basin to that of Somali Basin, which led to the triangular shape of the Mascarene and forced the Seychelles to rotate in an anticlockwise sense. Plummer & Belle (1995) assigns a late Cretaceous age for this rotation. The youngest unit sampled for palaeomagnetic analysis in this study is the microgranites where we obtained an $^{40}Ar/^{39}Ar$ age of 62.9 ± 0.7. This implies that the rotation must have occurred during or after the time of remanence acquisition, that is, from C28n during or after C27r. However, this does not rule out the possibility that this rotation could have started earlier. This additional information could fit very well in a tectonic scenario with active rifts/spreading centres at opposing corners of the microcontinent (this seems to be the case with the oceanic crust evolution around the Seychelles between chrons C30–C29 and C27). On a more detailed scale, the crust around the Seychelles shows evidence of deformation both to the north (just south of the oldest magnetic anomaly identified in the east Arabian Sea) and to the south where a rugged oceanic crust which was presumably formed in the Cretaceous Mascarene Basin suffered compression, as described by seismic and bathymetric data (see Masson 1984 and the bathymetric and free-air gravity signature; Fig. 9). More dramatically, the Amirante Ridge (a Cretaceous ridge located along a possible fracture zone SW of the Seychelles) has been described as an extinct trench that was formed as an incipient subduction zone (Miles 1982; Masson 1984; Mart 1988).

Based on earlier studies and our new results that indicate an anticlockwise rotation ($29.4^\circ \pm 12.9^\circ$) for the Seychelles sometime after magnetochron C28n, we propose that part of this rotation has been accommodated by propagating seafloor spreading in East Somali Basin, NW of Seychelles as documented by magnetic anomalies interpreted as C28n. After magnetochron C27r (when the Seychelles were isolated from the Laxmi Ridge by seafloor spreading) the Seychelles might have continued to rotate as an individual plate, therefore creating limited transpression and transtension along its plate boundaries. We note a series of fan-shaped features visible in bathymetry and free-air gravity NW and north of the Seychelles microcontinent (Fig. 9a, b). When reconstructed at chron 27n time, some of these features correspond to a small circle trend around a stage pole that depicts the anticlockwise rotation of Seychelles between C28n and C27n. This trend aligns well with the low in free-air gravity and trough in bathymetry and vintage seismic data (seismic line collected by Vema 1910 in 1963, published by Lamont Doherty Earth Observatory through GeoMapApp, http://www.geomapapp.org, and seismic line TCO-24, Plummer 1996) situated NW of Seychelles, and as a continuation of the Amirante Trough. A similar interpretation was suggested by Plummer (1996).

We cannot resolve the timing of the Amirante Ridge formation (as a compressional feature), but we emphasize that the rocks that have been described on Silhouette and the North Island on Seychelles have been suggested to be related to incipient subduction (Brown *et al.* 1984). A recent study (Calvès *et al.* 2011) suggests that a Mid–Late Cretaceous compressional event, caused by the relative motion between Madagascar and NW margin of India, led to the formation of the Amirante trench. The trench is suggested to be of age 82 ± 16 Ma from K/Ar analysis of a grab sample (Fisher *et al.* 1968) and formed some volcanic ridges along the western Indian margin.

A similar suggestion comes from a study on anisotropy of the lithosphere and upper mantle beneath Seychelles (Hammond *et al.* 2005). The observed large variation in the magnitude of shear-wave splitting is explained by a lithospheric structure that has been affected by a transpressive regime, possibly during the formation of the Mascarene Basin. If this is correct, then the Amirante Trench might

Fig. 9. (*Continued*) Seychelles microcontinent and fan-shaped lineations are shown in the inset figure, together with small circles around the Seychelles/India–Laxmi Ridge stage pole between 67.7 and 61 Ma (green curved lines). Note that the fan-shaped lineations are parallel or subparallel to the small circle trend that averages the anticlockwise rotation of the Seychelles microcontinent as suggested by the palaeomagnetic data. (**e**) A trough observed in the gravity data and on vintage seismic lines just NW of the Seychelles microcontinent might have been formed or affected by transform or transpressional motion generated by this rotation. Seismic profile (v1910) and location map are courtesy of Lamont Doherty Earth Observatory (LDEO) via the GeoMapApp application.

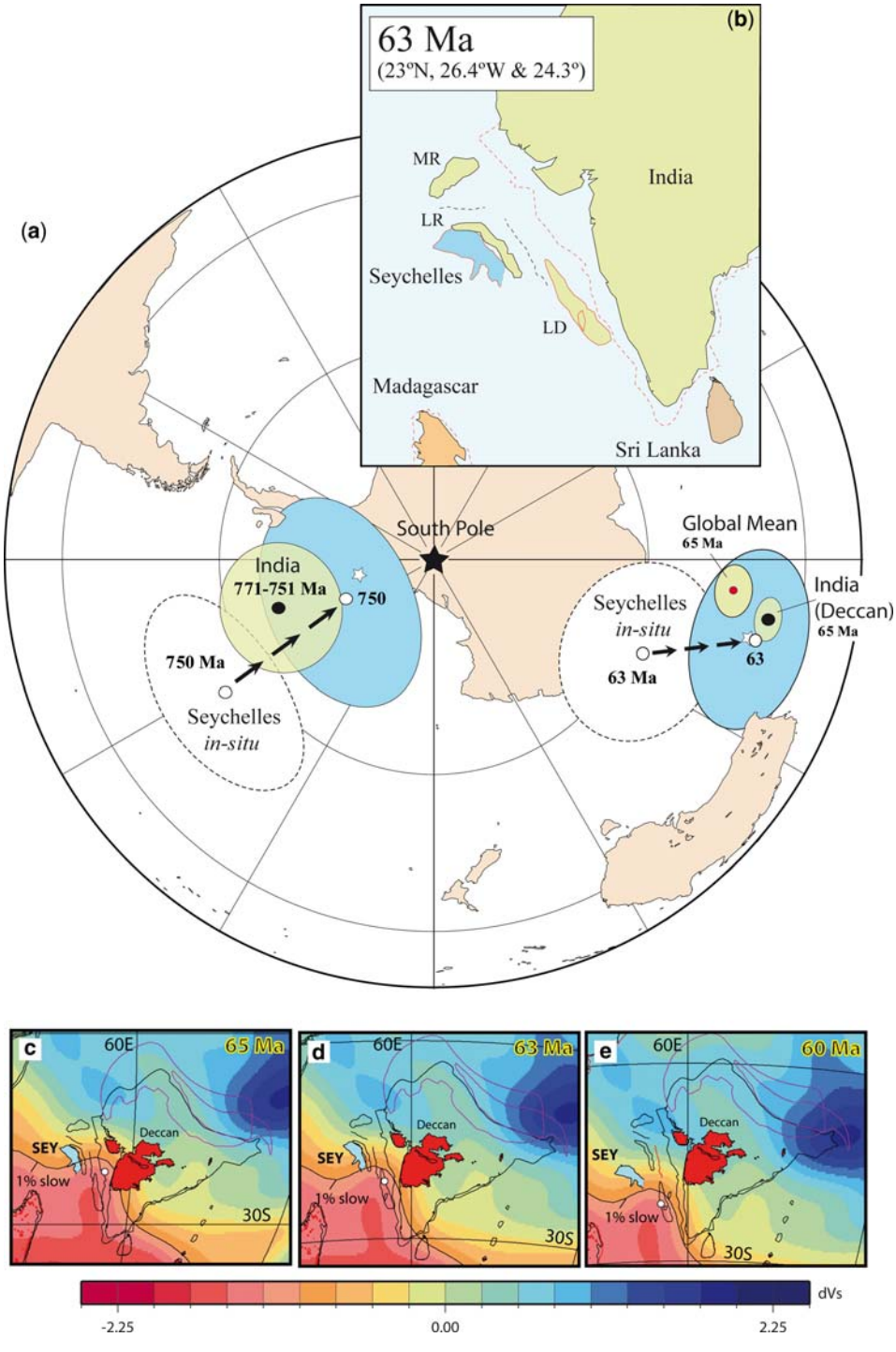

Fig. 10. (**a**) A comparison of the pole position derived from the present study (pole latitude −57.55°, longitude 114.22°, A95 = 12.2°) with a 65 Ma mean pole from India (essentially all from the Deccan Traps; latitutde 37.6°, longitude 100.2°, A95 = 3°, $N = 7$ poles) and a global 65 Ma mean pole (latitude −45.5°, longitude 96.1°, A95 = 3.5°, $N = 29$ poles) where all palaeomagnetic data were rotated to Indian co-ordinates and then averaged (Torsvik *et al.* 2008*c*).

have been formed in the Mid-Cretaceous but reactivated in the Paleocene due to the anticlockwise rotation of the Seychelles.

Stephens *et al.* (2009) provide a new insight into the origin of the Amirante ridge-trench. Geochemical and $^{40}Ar/^{39}Ar$ analysis on a gabbro sample, dredged from the southern tip of the arc, indicate a much younger age of 51.4 ± 0.9 Ma and their geochemical data largely rule out a subduction origin for the main phase of this structure. However, their explanation for the genesis of the Amirante trench as an impact crater remanent is refuted by the lack of evidences for strong unconformities that would have been observed in adjacent sedimentary basins (Plummer 1996).

A recent regional study by Cande *et al.* (2010) provides independent evidence for an anticlockwise rotation of the Seychelles microplate. By analysing large datasets of magnetic and fracture zone identifications, they predicted a plate boundary passing through the Amirante Ridge and extending north to the Carlsberg Ridge at least from C26y to C22o. However, they envisage that the independent motion of the Seychelles microplate might have started earlier (S. Cande, pers. comm. 2010).

Torsvik *et al.* (2001) proposed a fit of Seychelles and India at *c.* 750 Ma by matching Seychelles dykes and granites with the Malani pole of Klootwijk (1975). This fit (Euler pole latitude 25.8°N, longitude 30°W and rotation angle 28°) means that both the 750 Ma pole and our new 63 Ma pole (open stars in Fig. 10a) match contemporaneous mean poles from India within error (shown with green shaded A95 confidence oval). This reconstruction is very tight (probably more applicable to the Neoproterozoic); to account for pre-break-up extension along the Western margin of India (Fig. 10b), we therefore present a modified fit for the Early Paleocene (Euler pole latitude 23°N, longitude 26.4°W and rotation angle 28°). This fit also matches both the Neoproterozoic and Paleocene poles from the Seychelles (open white circles with blue shaded A95s). Our Seychelles pole also compares well with the global mean 65 Ma pole (red circle with green A95 oval). We also show the location of the Reunion hotspot (fixed with respect to the mantle) that is commonly linked to the Deccan Large Igneous Province (LIP). The reconstructions differs only by *c.* 4° in latitude compared to a global palaeomagnetic reference frame (Torsvik *et al.* 2008*b*), witnessing relatively little drift of the Reunion hotspot.

From cross-cutting relationship of dykes to formation ages in Western India, Hooper *et al.* (2010) argue that significant extension must have started during C29R (Fig. 4). There is also evidence that the intertrappean facies in the Mumbai area (Western India) had a ecosystem resembling a shallow brackish marine gulf environment by *c.* 64 Ma, with associated phreatomagmatic and spilitized flows (Cripps *et al.* 2005). This is in line with our reconstruction (Fig. 10b) where we maintain a tight fit between the Seychelles and the Laxmi Ridge (LR in Fig. 10b). We invoke rifting of both these domains from India between 70 and 65 Ma. After 63 Ma and the main Deccan Trap magmatism, the Seychelles separated from the Laxmi Ridge/India and rotated *c.* 25° anticlockwise during the initial separation. This is illustrated in Figure 10c–e where we reconstruct Seychelles–India from 65 to 60 Ma using an *absolute* Indo-Atlantic moving hotspot frame (O'Neill *et al.* 2005).

These reconstructions (Fig. 10c–e) are draped on shear-wave anomalies (Becker & Boschi 2002) near the core–mantle-boundary (CMB), assuming that these have been stable for several hundred million years (Torsvik *et al.* 2008*a*). Earlier work has demonstrated that practically all reconstructed LIPs of the past 300 Ma (Burke & Torsvik 2004; Torsvik *et al.* 2006, 2008*a*; Burke *et al.* 2008) or even >500 Ma (Torsvik *et al.* 2010) and active deep-plume sourced hotspots at the Earth's surface (Montelli *et al.* 2006) project radially down to a narrow stable plume generation zone on the CMB at the edge of the LLSVPs. The 1% slow velocity contour in the SMEAN (Becker & Boschi 2002) model is a fair approximation to the plume generation zones. Our reconstructions (Fig. 10c–e) confirm that India and the Seychelles lay nearly vertically about the Plume Generation Zone during the eruption of the Deccan Traps and that they can be linked to the active Reunion hotspot.

Conclusions

This work demonstrates that the Early Tertiary volcanic rocks of Seychelles were emplaced during magnetochron C28n. A weighted mean of several

Fig. 10. (*Continued*) We also compare a Neoproterozoic 750 Ma pole from the Seychelles (Torsvik *et al.* 2001; latitude −54.8°, longitude 96.1°, A95 = 3.5°, $N = 29$ poles) with a similar-aged pole from India, that is, the Malani Igneous Suite (Gregory *et al.* 2009); latitude −67.8°, longitude 252.5°, A95 = 8.8°). Unrotated (rotated) Seychelles means and 95% confidence ovals are shown as white (blue) colours. (**b**) Seychelles reconstructed. LR, MR and LD denote Laxmi Ridge, Murray Ridge and Lacadives. The Seychelles–Laxmi–Deccan Traps reconstructed. Reconstructions are shown for (**c**) 65 Ma, (**d**) 63 Ma and (**e**) 60 Ma and draped on shear-wave anomalies near the core–mantle-boundary. The 1% slow contour is shown with a black line.

samples from the North Island gave a $^{40}Ar/^{39}Ar$ age of 63.1 ± 0.34 Ma and a zircon weighted mean U–Pb age of 63.27 ± 0.05 Ma, pointing to a rapid cooling of this complex. The weighted mean U–Pb age obtained from the complex of Silhouette Island is 63.54 ± 0.06 Ma and are 0.27 ± 0.08 Ma older indicating a separate event. The $^{40}Ar/^{39}Ar$ results record a more prolonged time span with the trachytic tuffs giving an age of 66.8 ± 0.8 Ma, while the youngest unit (syenite) gave a weighted mean age of 61.3 ± 0.57 Ma. Some of these $^{40}Ar/^{39}Ar$ ages are distinguishable at the 95% confidence level.

The palaeomagnetic mean remanence direction implies that the Seychelles has rotated 29.4° ± 12.9° anticlockwise after their formation, some time after magnetochron C28n. The palaeomagnetic results from the Silhouette indicate that the magnetic remanence carries reverse polarity for all units apart from the microgranites. We observe that some rock units have recorded significant secular variation and that their place in the geomagnetic timescale (GTS2004) does not match the observed magnetic polarities. The difference between the U–Pb and $^{40}Ar/^{39}Ar$ age determinations and the mismatch with the geomagnetic timescale indicates that the volcanic complex of Silhouette experienced a protracted period of cooling.

The palaeomagnetic pole obtained in this study is 57.55°S and 114.22°E ($A95 = 12.3°$, $N = 14$) which, after correcting for the previously mentioned rotation, corresponds very well to poles of similar ages from the Deccan Traps.

Recent detailed studies of early Cenozoic kinematics independently confirmed the presence of a plate boundary between Seychelles and adjacent north and NW oceanic crust (Cande *et al.* 2010). We propose that part of this rotation has been accommodated while the Gop/Laxmi basins were formed north and NE of the Laxmi Ridge/Seychelles composite block, as our results suggest Seychelles motion during the postulated timing for the Gop rifting and seafloor spreading and early seafloor spreading of the East Somali Basin. After magnetochron C27r, when the Seychelles were isolated from the Laxmi Ridge by seafloor spreading, the Seychelles might have continued to rotate as an individual plate therefore creating transpression and transtension along its plate boundaries. This motion may have initiated subduction along the Amirante Trough, or reactivated an already weak zone affected by an earlier tectonic event.

Our palaeomagnetic results and new inferred ages of Seychelles volcanic rocks lead to a reconstructed volcanic region that lay nearly radially above the Plume Generation Zone during the eruption of the Deccan Traps and confirm a hotspot origin (possible Reunion) for this volcanic activity. In the light of recent debates around the timing and extent of the Deccan traps and the role of mantle plumes in relation to rifting of the Seychelles microcontinent (e.g. Sheth 2005; Collier *et al.* 2009; Armitage *et al.* 2010), our study shows that Seychelles volcanism occurred contemporaneously with the Deccan Trap volcanic emplacement and incipient seafloor spreading in the East Somali Basin.

Helpful and constructive reviews were provided by J. Collier and M. Widdowson. MG, DJJvH and THT appreciated funding from Statoil (Splates Project). CG acknowledges Scripps Institute of Oceanography for hosting her while working on the last version of the manuscript. We appreciate the editorial handling by S. Buiter. We thank Linda Vanherck and the staff at the North Island for providing access, guiding and help during sampling.

References

Allègre, C. J., Birck, J. L., Capmas, F. & Courtillot, V. 1999. Age of the Deccan traps using $^{187}Re-^{187}Os$ systematics. *Earth and Planetary Science Letters*, **170**, 197–204.

Amante, C. & Eakins, B. 2009. ETOPO1 1 Arc-minute global relief model: procedures, data sources and analysis, Technical Report, NOAA.

Armitage, J. J., Collier, J. S. & Minshull, T. A. 2010. The importance of rift history for volcanic margin formation. *Nature*, **465**, 913–917.

Ashwal, L. D., Demaiffe, D. & Torsvik, T. H. 2002. Petrogenesis of Neoproterozoic Granitoids and related rocks from the Seychelles: the case for an Andean-type arc origin. *Journal of Petrology*, **43**, 45–83.

Baker, B. H. 1963. Geology and mineral resources of the Seychelles Archipelago. *Geological Survey of Kenya Memoir*, **3**, 140.

Baksi, A. K. 2005. Comment on '$^{40}Ar/^{39}Ar$ dating of the Rajahmundry Traps, eastern India and their relations to the Deccan Traps' by Knight et al. [*Earth and Planetary Science Letters*, **208** (2003) 85–99]; *Earth and Planetary Science Letters*, **239**, 368–373.

Barron, E. J. & Harrison, C. G. A. 1980. An analysis of past plate motions the South Atlantic and Inian Oceans. *In*: Davies, P. & Runcorn, S. (eds) *Mechanisms of Plate Tectonics and Continental Drift*. Academic Press, New York, 89–110.

Basu, A. R., Renne, P. R., DasGupta, D. K., Teichmann, F. & Poreda, R. J. 1993. Early and Late Alkali Igneous Pulses and a High-^{3}He Plume Origin for the Deccan Flood Basalts. *Science*, **261**, 902–906.

Becker, W. & Boschi, L. 2002. A comparison of tomographic and geodynamic mantle models. *Geochemistry, Geophysics, Geosystems*, **3**, 1003.

Bernard, A. & Munschy, M. 2000. Le bassin des Mascareignes et le bassin de Laxmi (ocean Indien

occidental) se sont-ils formes a l'axe d'un meme centre d'expansion? *Sciences de la Terre et Des Planetes*, **330**, 777–783.

Beyene, A. & Abdelsalam, M. G. 2005. Tectonics of the Afar Depression: a review and synthesis. *Journal of African Earth Sciences*, **41**, 41–59.

Bhattacharya, G. C., Chaubey, A. K., Murty, G. P. S., Srinivas, K., Sarma, K. V. L. N. S., Subrahmanyam, V. & Krishna, K. S. 1994. Evidence for seafloor spreading in the Laxmi Basin, northeastern Arabian sea. *Earth and Planetary Science Letters*, **125**, 211–220.

Biggin, A., van Hinsbergen, D. J. J., Langereis, C. G., Straathof, G. B. & Deenen, M. H. 2008. Geomagnetic secular variation in the Cretaceous Normal Superchron and in the Jurassic. *Physics of the Earth and Planetary Interiors*, **169**, 3–19.

Brown, G. C., Thorpe, R. S. & Webb, P. C. 1984. The geochemical characteristics of granitoids in constrasting arcs and comments on magma sources. *Journal of the Geological Society, London*, **141**, 413–426.

Burke, K. & Torsvik, T. H. 2004. Derivation of Large Igneous Provinces of the past 200 million years from long-term heterogeneities in the deep mantle. *Earth and Planetary Science Letters*, **227**, 531–538.

Burke, K., Steinberger, B., Torsvik, T. H. & Smethurst, M. A. 2008. Plume Generation Zones at the margins of Large Low Shear Velocity Provinces on the core–mantle boundary. *Earth and Planetary Science Letters*, **265**, 49–60.

Butler, R. F. 1992. *Paleomagnetism: Magnetic Domains to Geologic Terranes*. Blackwell Scientific Publications, Boston.

Calvès, G., Clift, P. D. & Inam, A. 2008. Anomalous subsidence on the rifted volcanic margin of Pakistan: no influence from Deccan plume. *Earth and Planetary Science Letters*, **272**, 231–239.

Calvès, G., Schwab, A. M. *et al.* 2011. Seismic volcanostratigraphy of the Western Indian rifted margin: the pre-Deccan Igneous Province. *Journal of Geophysical Research*, **116**, B01101, doi: 10.1029/2010JB000862.

Cande, S. C., Patrait, P. & Dyment, J. 2010. Motion between the Indian, Antarctic and African plates in the early Cenozoic. *Geophysical Journal International*, **183**, 127–149.

Chaubey, A. K., Gopala Rao, D., Srinivas, K., Ramprasad, T., Ramana, M. V. & Subrahmanyam, V. 2002. Analyses of multichannel seismic reflection, gravity and magnetic data along a regional profile across the central-western continental margin of India. *Marine Geology*, **182**, 303–323.

Chenet, A., Quidelleur, X., Fluteau, F., Courtillot, V. & Bajpai, S. 2007. 40 K–40 Ar dating of the Main Deccan large igneous province: further evidence of KTB age and short duration. *Earth and Planetary Science Letters*, **263**, 1–15.

Cherniak, D. J. & Watson, E. B. 2001. Pb diffusion in zircon. *Chemical Geology*, **177**, 5–24.

Coffin, M. F. & Rabinowitz, P. D. 1988. *Evolution of the conjugate East African–Madagascan margins and the western Somali Basin*. Geological Society of America Special Papers, **226**.

Coffin, M. F. & Eldholm, O. 1992. Volcanism and continental break-up: a global compilation of large igneous provinces. *In*: Storey, B. C., Alabaster, T. & Pankhurst, R. J. (eds) *Magmatism and the Causes of Continental Break-up*. Geological Society, London, Special Publications, **68**, 17–30.

Collier, J. S., Sansom, V., Ishizuka, O., Taylor, R. N., Minshull, T. A. & Whitmarsh, R. B. 2008. Age of Seychelles–India break-up. *Earth and Planetary Science Letters*, **272**, 264–277.

Collier, J. S., Minshull, T. A. *et al.* 2009. Factors influencing magmatism during continental breakup: new insights from a wide-angle seismic experiment across the conjugate Seychelles–Indian margins. *Journal of Geophysical Research*, **114**, B03101.

Corfu, F. 2004. U–Pb age, setting, and tectonic significance of the anorthosite–mangerite–charnockite–granite-suite, Lofoten-Vesterålen, Norway. *Journal of Petrology*, **45**, 1799–1819, doi: 10.1093/petrology/egh034.

Corfu, F. 2009. When the CA-TIMS therapy fails: the over-enthusiastic, the mixed-up, and the stubborn zircon. AGU Fall Meeting, Abstract V53B-05.

Courtillot, V. E. & Renne, P. R. 2003. On the ages of flood basalt events. *Comptes Rendus Geosciences*, **335**, 113–140.

Courtillot, V., Besse, J., Vandamme, D., Montigny, R., Jaeger, J. J. & Cappetta, H. 1999. Deccan flood basalts at the Cretaceous/Tertiary boundary? *Memoir – Geological Society of India*, **43**(Part 1), 173.

Cox, A. 1969. Confidence limits for the precision parameter k. *Geophysical Journal International*, **17**, 545–549.

Cripps, J. A., Widdowson, M., Spicer, R. A. & Jolley, D. W. 2005. Costal ecosystem responses to late stage Deccan Trap volcanism: the post K–T boundary (Danian) palynofacies of Mumbai (Bombay), west India. *Palaeogeography, Palaeoclimatology, Palaeoecology*, **216**, 303–332.

Crowley, J. L., Bowring, S. A. & Hanchar, J. M. 2006. What is a magma crystallization age? Insight from micro-sampling of chemical domains in zircon from the Fish Canyon Tuff. *Geochimica et Cosmochimica Acta*, **70**, A120.

Day, R., Fuller, M. & Schmidt, V. A. 1977. Hysteresis properties of titanomagnetites: grain-size and compositional dependence. *Physics of Earth and Planetary Science Letters*, **13**, 260–267.

Deenen, M. H., Langereis, C. G. & van Hinsbergen, D. J. J. 2011. Geomagnetic secular variation and the statistics of palaeomagnetic directions. *Geophysical Journal International*, doi: 10.1111/j.1365-246X.2011.05050.x.

Devey, C. W. & Stephens, W. E. 1991. Tholeiitic dykes in the Seychelles ant eh original spatial extent of the Deccan. *Journal of Geological Society, London*, **148**, 979–983.

Dickin, A. P., Fallick, A. E., Halliday, A. N., Macintyre, R. M. & Stephens, W. E. 1986. An isotopic and geochronological investigation of the younger igneous rocks of the Seychelles microcontinent. *Earth and Planetary Science Letters*, **81**, 46–56.

Duncan, R. A. 1990. The volcanic record of the Reunion hotspot. *In*: Duncan, R. A., Backman, J., Dunbar, R.

B. & PETERSON, L. G. (eds) *Proceedings of the Ocean Drilling Project, Scientific Results*, **115**, Ocean Drilling Program, Texas A and M University, 3–10.

FISHER, N. I. 1953. Dispersion on a sphere. *Proceedings of the Royal Society of London*, **A217**, 295–305.

FISHER, N. I., LEWIS, T. & EMBLETON, B. J. J. 1987. *Statistical Analysis of Spherical Data*. Cambridge University Press, Cambridge.

FISHER, R. L., ENGEL, C. G. & HILDE, T. W. 1968. Basalts dredged from the Amirante Ridge, western Indian Ocean. *Deep-Sea Research*, **15**, 521–534.

GAINA, C., GERNIGON, L. & BALL, P. 2009. Paleocene–Recent Plate Boundaries in the NE Atlantic and the formation of Jan Mayen microcontinent. *Journal of Geological Society*, **166**, 601–616, doi: 10.1144/0016-76492008-112.

GAINA, C., MÜLLER, R. D., BROWN, B., ISHIHARA, T. & IVANOV, S. 2007. Breakup and early seafloor spreading between India and Antarctica. *Geophysical Journal International*, **170**, 151–169.

GREGORY, L. C., MEERT, J. G., BINGEN, B., PANDIT, M. K. & TORSVIK, T. H. 2009. Paleomagnetism and geochronology of the Malani Igneous Suite, Northwest India: Implications for the configuration of Rodinia and the assembly of Gondwana. *Precambrian Research*, **170**, 13–26.

HALLIMOND, A. F. & HERROUN, E. F. 1933. Laboratory determinations of the magnetic properties of certain igneous rocks. *Proceedings of the Royal Society of London*, **141**, 302–314.

HAMMOND, J. O. S., KENDALL, J. *ET AL.* 2005. Upper mantle anisotropy beneath the Seychelles microcontinent. *Journal of Geophysical Research*, **110**, B11401, doi: 10.1029/2005JB003757.

HOOPER, P., WIDDOWSON, M. & KELLY, S. 2010. Tectonic setting and timing of the final Deccan flood basalt eruptions. *Geology*, **38**, 839–842, doi: 10.1130/G31072.1.

JAFFEY, A. H., FLYNN, K. F., GLENDENIN, L. E., BENTLEY, W. C. & ESSLING, A. M. 1971. Precision measurement of half-lives and specific activities of 235U and 238U. *Physical Review, Section C, Nuclear Physics*, **4**, 1889–1906.

JAY, A. E. & WIDDOWSON, M. 2008. Stratigraphy, structure and volcanology of the SE Deccan continental flood basalt province: implications for eruptive extend and volumes. *Journal of Geological Society, London*, **165**, 177–188.

JAY, A. E., MAC NIOCAILL, C., WIDDOWSON, M., SELF, S. & TURNER, W. 2009. Deccan flood basalt province, India: implications for the volcanostratigraphic architecture of continental flood basalt provinces. *Journal of Geological Society, London*, **166**, 13–24.

JOHNSON, C. L., CONSTABLE, C. G. *ET AL.* 2008. Recent investigations of the 0–5 Ma geomagnetic field recorded by lava flows. *Geochemistry, Geophysics, Geosystems*, **9**, Q04032.

KENT, J. T., BRIDEN, J. C. & MARDIA, K. V. 1983. Linear and planar structure in ordered multivariate data as applied to progressive demagnetisation of palaeomagnetic remanence. *Geophysical Journal of the Royal Astronomical Society*, **81**, 75–87.

KHRAMOV, A. N. 1958. Palaeomagnetism and stratigraphic correlation. *In*: IRVING, E. (ed.) *Paleomagnetism and its Application to Geological and Geophysical Problems*. 1st edn. Wiley, New York.

KLOOTWIJK, C. T. 1975. A note on the Palaeomagnetism of the late precambrian malani rhyolites near Jodhpur – India. *Journal of Geophysics*, **41**, 189–200.

KÖNIG, M. & JOKAT, W. 2006. The Mesozoic breakup of the Weddell Sea. *Journal of Geophysical Research*, **111**, B12102, doi: 10.1029/2005JB004035.

KRISHNA, K. S., GOPALA RAO, D. & SAR, D. 2006. Nature of the crust in the Laxmi Basin (14° –20°N), western continental margin of India. *Tectonics*, **25**, 1–18.

KROGH, T. E. 1973. A low contamination method for hydrothermal decomposition of zircon and extraction of U and Pb for isotopic age determinations. *Geochimica et Cosmochimica Acta*, **37**, 485–494.

KROGH, T. E. 1982. Improved accuracy of U–Pb zircon ages by the creation of more concordant systems using an air abrasion technique. *Geochimica et Cosmochimica Acta*, **46**, 637–649.

LANE, C. I. 2006. *Rifted margin formation in the northwest Indian Ocean: the extensional and magmatic history of the Laxmi Ridge continental margin*. Ph.D. thesis, University of Southampton.

LUDWIG, K. R. 2003. Isoplot 3.0. *A Geochronological Toolkit for Microsoft Excel*. Berkeley Geochronology Center Special Publication No. 4.

MAHONEY, J., NICOLLET, C. & DUPUY, C. 1991. Madagascar basalts: tracking oceanic and continental sources. *Earth and Planetary Science Letters*, **104**, 350–363.

MAUS, S., LUEHR, H., MARTIN, R., HEMANT, K., BALASIS, G., RITTER, P. & CLAUDIA, S. 2007. Fifth-generation lithospheric magnetic field model from CHAMP satellite measurements. *Geochemistry, Geophysics, Geosystems*, **8**, Q05013, doi: 10.1029/2006GC001521.

MART, Y. 1988. The tectonic setting of the Seychelles, Mascarene and Amirante plateaus in the western equatorial Indian Ocean. *Marine Geology*, **79**, 261–274.

MASSON, D. G. 1984. Evolution of the Mascarene Basin, western Indian Ocean, and the significance of the Amirante Arc. *Marine Geophysics Research*, **6**, 365–382.

MATTINSON, J. M. 2005. Zircon U–Pb chemical abrasion ('CA-TIMS') method: combined annealing and multi-step partial dissolution analysis for improved precision and accuracy of zircon ages. *Chemical Geology*, **220**, 47–66.

MCDOUGALL, I. & HARRISON, T. M. 1999. *Geochronology and Thermochronology by the $^{40}Ar/^{39}Ar$ Method*. 2nd edn. Oxford University Press, New York.

MCFADDEN, P. L. & MCELHINNY, M. W. 1988. The combined analysis of remagnetization circles and direct observations in palaeomagnetism. *Earth and Planetary Science Letters*, **87**, 161–172.

MCFADDEN, P. L., MERRILL, R. T., MCELHINNY, M. W. & SUNHEE, L. 1991. Reversals of the earth's magnetic field and temporal variations of the dynamo families. *Journal of Geophysical Research*, **96**, 3923–3933.

MCKENZIE, D. & SCLATER, J. G. 1971. The evolution of the Indian Ocean since the Late Cretaceous. *Geophysical Journal of the Royal Astronomical Society*, **25**, 437–528.

MILES, P. R. 1982. Gravity models of the Amirante Arc, western Indian Ocean. *Earth and Planetary Science Letters*, **61**, 127–135.

MILLER, J. S., MATZEL, J. E. P., MILLER, C. F., BURGESS, S. D. & MILLER, R. B. 2007. Zircon growth and recycling during the assembly of large, composite arc plutons. *Journal of Volcanology Geothermal Research*, **167**, 282–299.

MINSHULL, T. A., LANE, C. I., COLLIER, J. S. & WHITMARSH, R. B. 2008. The relationship between rifting and magmatism in the northeastern Arabian Sea. *Nature Geoscience*, **1**, 463–467.

MITCHELL, C. & WIDDOWSON, M. 1991. A geological map of the southern Deccan Traps, India and its structural implications. *Journal of the Geological Society, London*, **148**, 495–505.

MONTELLI, R., NOLET, G., DAHLEN, F. A. & MASTERS, G. 2006. A catalogue of deep mantle plumes: new results from finite-frequency tomography. *Geochemistry, Geophysics, Geosystems*, **7**, (Q11007).

NORTON, I. O. & SCLATER, J. G. 1979. A model for the evolution of the Indian Ocean and the break-up of Gondwanaland. *Journal of Geophysical Research*, **84**, 6803–6830.

OGG, J. G. & SMITH, A. G. 2004. The geomagnetic polarity time scale. *In*: GRADSTEIN, F. M., OGG, J. G. & SMITH, A. G. (eds) *A Geologic Time Scale 2004*. Cambridge University Press, Cambridge, 63–86.

O'NEILL, C., MÜLLER, R. D. & STEINBERGER, B. 2005. On the uncertainties in hotspot reconstructions, and the significance of moving hotspot reference frames. *Geochemistry, Geophysics, Geosystems*, **6**, Q04003.

PLUMMER, P. S. 1995. Ages and geological significance of the igneous rocks from Seychelles. *Journal of African Earth Sciences*, **20**, 91–101.

PLUMMER, P. S. 1996. The Amirante ridge/trough complex: response to rotational transform rift/drift between Seychelles and Madagascar. *Terra Nova*, **8**, 34–47.

PLUMMER, P. S. & BELLE, E. R. 1995. Mesozoic tectono-stratigraphic evolution of the Seychelles microcontinent. *Sedimentary Geology*, **96**, 73–91.

RENNE, P. R., SWISHER, C. C., DEINO, A. L., KARNER, D. B., OWENS, T. L. & DEPAOLO, D. J. 1998. Intercalibration of standards, absolute ages and uncertainties in $^{40}Ar/^{39}Ar$ dating. *Chemical Geology*, **145**, 117–152.

ROYER, J.-Y., CHAUBEY, A. K., DYMENT, J., BHATTACHARYA, G. C., SRINIVAS, K., YATHEESH, V. & RAMPRASAD, T. 2002. Paleogene plate tectonic evolution of the Arabian and Eastern Somali basins. *In*: CLIFT, P. D., KROON, D., GAEDICKE, C. & CRAIG, J. (eds) *The Tectonic and Climatic Evolution of the Arabian Sea Region*. Geological Society, London, Special Publications, **195**, 7–23.

SANDWELL, D. T. & SMITH, W. H. F. 1997. Marine gravity anomaly from Geosat and ERS-1 satellite altimetry. *Journal of Geophysical Research*, **102**, 10 039–10 050.

SCHÄRER, U. 1984. The effect of initial 230Th disequilibrium on young U–Pb ages: the Makalu case, Himalaya. *Earth and Planetary Science Letters*, **67**, 191–204.

SCHOENE, B., CROWLEY, J. L., CONDON, D. J., SCHMITZ, M. D. & BOWRING, S. A. 2006. Reassessing the uranium decay constants for geochronology using ID-TIMS U–Pb data. *Geochimica et Cosmochimica Acta*, **70**, 426–445.

SELF, S., JAY, A. E., WIDDOWSON, M. & KESZTHELYI, L. P. 2008. Correlation of the Deccan and Rajahmundry Trap lavas: are these the longest and largest lava flows on Earth? *Journal of Volcanology and Geothermal Research*, **172**, 3–19.

SHETH, H. C. 2005. From Deccan to Reunion: no trace of a mantle plume. *In*: FOULGER, G. R., NATLAND, J. H., PRESNALL, D. C. & ANDERSON, D. L. (eds) *Plates, Plumes and Paradigms Geological Society of America*. Geological Society of America Special Papers, **388**, Boulder, Colorado, 477–501.

SHETH, H. C., PANDE, K. & BHUTANI, R. 2001. $^{40}Ar–^{39}Ar$ Ages of Bombay Trachytes: evidence for a Palaeocene phase of Deccan Volcanism. *Geophysical Research Letters* **28**, 3513–3516.

SMITH, W. H. F. & SANDWELL, D. T. 1997. Global seafloor topography from satellite altimetry and ship depth soundings. *Science*, **277**, 1957–1962.

STEIGER, R. H. & JÄGER, E. 1977. Subcommission on geochronology: Convention on the use of decay constants in geo- and cosmochronology. *Earth and Planetary Science Letters*, **36**, 359–362.

STEPHENS, W. E. & DEVEY, C. M. 1992. Seychelles and the fragmentation of Gondwana: evidence from the igneous rocks. *In*: PLUMMER, S. (ed.) *Proceedings of the First Indian Ocean Regional Seminar on Petroleum Exploration*, Seychelles. Seychelles National Oil Company (69), Victoria, Seychelles, 211–222.

STEPHENS, W. E., STOREY, M., DONALDSON, C. H., ELLAM, R. M., LELIKOV, E., TARARIN, G. & GARBE-SCHONENBERG, C. 2009. Age and origin of the Amirante ridge-trench structure, western Indian Ocean. *In*: *Proceedings of Fall Meeting of American Geophysical Union*, abstract #T23A-1885.

STOREY, M., MAHONEY, J. J., SAUNDERS, A. D., DUNCAN, R. A., KELLEY, S. P. & COFFIN, M. F. 1995. Timing of hot spot-related volcanism and the break-up of Madagascar and India. *Science*, **267**, 852–855.

STOREY, M., MAHONEY, J. J. & SAUNDERS, A. D. 1997. Cretaceous basalts in Madagascar and the transition between plume and continental lithosphere mantle sources. *In*: MAHONEY, J. J. & COFFIN, M. F. (eds) *Large Igneous Provinces: Continental, Oceanic, and Planetary Flood Volcanism*. American Geophysical Union, Washington, Geophysical Monograph, 95–122.

SUBRAHMANYAM, V., RAO, D. G., RAMANA, M. V., KRISHNA, K. S., MURTY, G. P. S. & GANGADHARARAO, M. 1995. Structure and tectonics of the southwestern continental margin of India. *Tectonophysics*, **249**, 267–282.

TAUXE, L. & KENT, D. V. 2004. A simplified statistical model for the geomagnetic field and the detection of shallow bias in paleomagnetic inclinations: was the ancient magnetic field dipolar? *In*: CHANNEL, J. E. T., KENT, D. V., LOWRIE, W. & MEERT, J. G. (eds) *Timescales of the Paleomagnetic Field*. American Geophysical Union, Washington, Geophysical Monograph, **145**, 101–116.

TAUXE, L., KODAMA, K. P. & &KENT, D. V. 2008. Testing corrections for paleomagnetic inclination error in sedimentary rocks: a comparative approach. *Physics of the Earth and Planetary Interiors*, **169**, 152–165.

TODAL, A. & ELDHOLM, O. 1998. Continental margin off Western India and Deccan Large Igneous Province. *Marine Geophysical Researches*, **20**, 273–291.

TORSVIK, T. H., TUCKER, R. D., ASHWAL, L. D., EIDE, E. A., RAKOTOSOLOFO, N. A. & DE WIT, M. J. 1998. Late Cretaceous magmatism in Madagascar: palaeomagnetic evidence for a stationary Marion hotspot. *Earth and Planetary Science Letters*, **164**, 221–232.

TORSVIK, T. H., BRIDEN, J. C. & SMETHURST, M. A. 2000. Super-IAPD Interactive analysis of palaeomagnetic data. www.Geodynamics.no/software.Htm.2009.

TORSVIK, T. H., ASHWAL, L. D., TUCKER, R. D. & EIDE, E. A. 2001. Geochronology and palaeogeography of the Seychelles microcontinent: the India link. *Precambrian Research*, **100**, 47–59.

TORSVIK, T. H., SMETHURST, M. A., BURKE, K. & STEINBERGER, B. 2006. Large igneous provinces generated from the margins of the large low-velocity provinces in the deep mantle. *Geophysics Journal International*, **167**, 1447–1460.

TORSVIK, T. H., SMETHURST, M. A., BURKE, K. & STEINBERGER, B. 2008*a*. Long term stability in deep mantle structure: evidence from the ~300 Ma Skagerrak-Centered Large Igneous Province (the SCLIP). *Earth and Planetary Science Letters*, **267**, 444–452.

TORSVIK, T. H., STEINBERGER, B., COCKS, L. R. M. & BURKE, K. 2008*b*. Longitude: linking Earth's ancient surface to its deep interior. *Earth and Planetary Science Letters*, **276**, 273–282.

TORSVIK, T. H., MÜLLER, R. D., VAN DER VOO, R., STEINBERGER, B. & GAINA, C. 2008*c*. Global Plate Motion Frames: Toward a unified model. *Reviews of Geophysics*, **46**, RG3004.

TORSVIK, T. H., BURKE, K., WEBB, S., ASHWAL, L. & STEINBERGER, B. 2010. Diamonds sampled by plumes from the core–mantle boundary. *Nature*, **466**, 352–355, doi:10.1038/nature09216.

TUCKER, R. D., ASHWAL, L. D. & TORSVIK, T. H. 2001. U–Pb geochronology of Seychelles granitoids: a Neoproterozoic continental arc fragment. *Earth and Planetary Science Letters*, **187**, 27–38.

VANDAMME, D. 1994. A new method to determine paleosecular variation. *Physics of the Earth and Planetary Interiors*, **85**, 131–142.

VAN HINSBERGEN, D. J. J., STRAATHOF, G. B., KUIPER, K. F., CUNNINGHAM, W. D. & WIJBRANS, J. R. 2008*a*. No rotations during transpressional orogeny in the Gobi Altai: coinciding Mongolian and Eurasian apparent polar wander paths. *Geophysical Journal International*, **173**, 105–126.

VAN HINSBERGEN, D. J. J., DUPONT-NIVET, G., NAKOV, R., OUD, K. & PANAIOTU, C. 2008*b*. No significant post-Eocene rotation of the Moesian Platform and Rhodope (Bulgaria): implications for the kinematic evolution of the Carpathian and Aegean arcs. *Earth and Planetary Science Letters*, **273**, 345–358.

VELAIN, C. 1879. Notes sur la constitution geologique des Iles Seychelles. *Bulletin de la Societe Geologique de France*, **7**, 278.

WENSINK, H. 1973. Newer paleomagnetic results of the Deccan Traps, India. *Tectonophysics*, **17**, 41–59.

WENSINK, H., BOELRIJK, N. A. I. M., HEBEDA, E. H., PRIEM, H. N. A., VERDURMEN, E. A. T. & VERSCHURE, R. H. 1977. Paleomagnetism and radiometric age determinations of the Deccan Traps, India. *IV International Gondwana Symposium*, Calcutta (India). Hindustan Publishing Corporation, Delhi (India). 832–849.

YATHEESH, V., BHATTACHARYA, G. C. & DYMENT, J. 2009. Early oceanic opening off Western India–Pakistan margin: The Gop Basin revisited. *Earth and Planetary Science Letters*, **284**, 399–408.